Chapter 6
Interatomic Potentials, Scattering and Nuclear Stopping

Abstract This chapter focuses on interatomic potentials of interest in single and multiple scattering of heavy charged particles and the associated energy loss. In the keV energy range and above it is commonly assumed that binary elastic scattering on central potentials makes up an adequate description. Limitations of this description are mentioned. Classical scattering for screened-Coulomb interaction is outlined, and special attention is given to scaling properties, in particular for Thomas-Fermi-type interaction. Power-law scattering is mentioned as a convenient tool for rough estimates. Comparisons between different theoretical estimates as well as between measured and calculated cross sections are presented, and attempts to directly invert a measured cross section into the underlying potential are reported. The chapter concludes with explicit results for nuclear stopping and straggling including pertinent experiments.

6.1 Introductory Comments

Elements of classical and quantal scattering theory for central-force potentials have been presented in Chap. 3, Vol. 1, with applications mainly to Coulomb interaction between point charges. The present chapter addresses interactions between screened ions and atoms as well as between neutral atoms. In the field of radiation physics such screened-Coulomb forces are most often expressed in terms of central pairwise potentials, but more sophisticated descriptions may be appropriate, in particular for collisions at energies in the eV and lower-keV range.

A simple estimate presented in Sect. 2.3, Vol. 1 suggests the stopping cross section for electronic collisions to exceed that for elastic nuclear collisions by 3–4 orders of magnitude. This result holds for interactions between practically free point charges within an energy regime where stopping cross sections decrease monotonically with increasing energy. You have seen in Chap. 4 that the electronic stopping cross section actually experiences a maximum and, from there, decreases monotonically toward zero with decreasing energy. We shall see that the nuclear stopping

P. Sigmund, *Particle Penetration and Radiation Effects Volume 2*,
Springer Series in Solid-State Sciences 179, DOI: 10.1007/978-3-319-05564-0_6,

cross section exhibits a similar behaviour, but at a lower energy and with a different height. In general there exists a cross-over point between electronic and nuclear stopping at some energy which, for not too light ions, lies in the keV or lower-MeV range. For collision cascades governing radiation effects such as defect formation and sputtering, discussed briefly in Chap. 1, Vol. 1, nuclear stopping is most often the dominating process.

At higher beam energies, where electronic stopping dominates energy loss, angular deflections are governed by the interaction with the nuclei, as you have seen in Chap. 2, Vol. 1. For small-angle deflections—which determine multiple scattering—it is essential that screening of the interaction be taken properly into account.

6.2 Potentials

Calculating the interaction force between two (neutral or charged) atoms is in principle a problem of quantum chemistry, but the type of questions asked in radiation physics is different from standard problems treated in quantum chemistry. Most of all, the range of internuclear distances of interest in scattering problems differs from that in molecular physics: Atoms moving with kinetic energies in the keV regime or above may approach each other to internuclear distances much smaller than those of atoms bound in a molecule. From this follows that interaction forces of interest are predominantly repulsive, while in traditional quantum chemistry it is more the equilibrium range that is of interest.

Moreover, the range of relative velocities of interacting atoms may lie several orders of magnitude above what is of interest in molecular spectroscopy and chemical reaction kinetics. In quantum chemistry and molecular-beam physics, adiabatic potentials, based on the ground-state configuration of the combined electron cloud of two collision partners, are typically a good first estimate. Conversely, once the relative speed between the colliding nuclei exceeds characteristic orbital velocities of the target and projectile electrons, it may be more appropriate to consider the opposite extreme, ignore any deformation of the electron clouds during collision and, instead, determine the interaction between undisturbed atomic-electron configurations.

Within the scope of this book, more emphasis will be laid on general behaviour than on element-specific details. Therefore, scaling laws valid for a wide range of elements and their experimental verification will receive attention. This, in fact, is dictated by necessity: There are about 10^4 ion-target systems if only atomic beams and elemental targets are taken into consideration. If molecular and cluster beams are allowed for as well as alloyed and compound targets, the variety of systems to be treated *ab initio* becomes rapidly prohibitive from the point of view of computational capacity and manpower.

The main justification of various adopted screening functions and screening radii is their ability to accurately describe pertinent experimental results. Those include measurements of elastic ion-atom scattering distributions under single- and/or

multiple-collision conditions as well as range distributions of ions in solids. Experiments in the former category will be mentioned later in this chapter, whereas the physics of ion ranges will be the subject of Chap. 9.

6.2.1 Bohr's Estimate

Bohr (1948) presented a first estimate of the interaction potential between two atoms on the basis of the electrostatic interaction energy of two stiff charge distributions,

$$\mathcal{V}(R) = -e \int \mathrm{d}^3\boldsymbol{r}\, \rho_1(\boldsymbol{r})\Phi_2(\boldsymbol{r})\,, \tag{6.1}$$

where $\rho_1(\boldsymbol{r}) = \rho_1(r_1)$ and $\phi_2(\boldsymbol{r}) = \phi_2(r_2)$ denote the charge density and electrostatic potential of the respective collision partners,

$$r_1 = |\boldsymbol{r} - \boldsymbol{R}_1| \quad r_2 = |\boldsymbol{r} - \boldsymbol{R}_2| \tag{6.2}$$

and $R = |\boldsymbol{R}_1 - \boldsymbol{R}_2|$ their internuclear distance. Yukawa-type charge distributions were assumed with Thomas-Fermi-type screening radii

$$a_1 = \frac{a_0}{Z_1^{1/3}}; \quad a_2 = \frac{a_0}{Z_2^{1/3}}\,. \tag{6.3}$$

You are encouraged to determine $\mathcal{V}(R)$ by solving Problem 6.1. If both collision partners are neutral atoms, the result is

$$\mathcal{V}(R) = \frac{Z_1 Z_2 e^2}{R}\, g(R) \tag{6.4}$$

$$g(R) = \frac{a_2^2 \mathrm{e}^{-R/a_1} - a_1^2 \mathrm{e}^{-R/a_2}}{a_2^2 - a_1^2}. \tag{6.5}$$

Equation (6.5) has been plotted in Fig. 6.1 for a series of values of the ratio a_1/a_2. The distance R is taken relative to the Bohr screening radius defined by

$$\frac{1}{a^2} = \frac{1}{a_1^2} + \frac{1}{a_2^2}\,. \tag{6.6}$$

As you could expect, for large values of a_1/a_2, atom 1 acts similar to a point charge, so that curves approach Bohr's expression

$$g(R) = \mathrm{e}^{-R/a}\,. \tag{6.7}$$

Scaling with a according to (6.6) is obeyed approximately for $R/a \lesssim 1$, but increasing differences are seen in the tails.

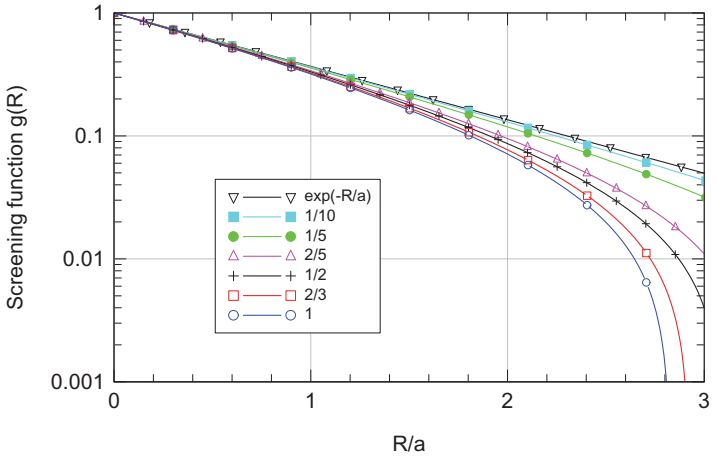

Fig. 6.1 Screening function $g(R)$ of the interaction potential between two neutral atoms according to (6.5). Numbers in the legend refer to different values of a_1/a_2. The solid curve refers to Bohr's estimate, (6.7)

The potential used in a series of papers by Lindhard and coworkers, especially Lindhard et al. (1968), differs from Bohr's estimate in two respects,

- The exponential screening function was replaced by the neutral-atom screening function either for the Thomas-Fermi or the Lenz-Jensen atom discussed in Sect. 1.4.4, and
- The screening radius was replaced by the $a_j = 0.8853a_0/Z_j^{1/3}$.

Figure 6.1 refers to the interaction between two neutral atoms. In the literature you will see potentials of this type also applied to interactions between positively and even negatively charged ions and atoms. This is plausible for not too highly-charged ions, since substantial deflection and/or energy transfer in elastic collisions implies impact parameters smaller than outer-shell radii.

To study this point further, you may use the result of Problem 6.1 which, for a nonvanishing ion charge $q_1 e$, yields a screening function

$$g(R) = \frac{1}{1 - a_1^2/a_2^2}\left[\left(1 - \frac{q_1}{Z_1}\right)\mathrm{e}^{-R/a_1} + \left(\frac{q_1}{Z_1} - \frac{a_1^2}{a_2^2}\right)\mathrm{e}^{-R/a_2}\right]. \qquad (6.8)$$

For a meaningful plot you need to make some assumptions on the dependence of the screening radius a_1 on the ion charge. This can be done by matching the screening functions shown in Fig. 1.8 by an exponential

$$g(r/a) \simeq (1 - q/Z)\mathrm{e}^{-r/a}\,. \qquad (6.9)$$

Within the accuracy of an exponential fit to the potential we may write (Sigmund, 1997)

$$a \simeq a_{\mathrm{TF}}(1 - q/Z)^{\alpha}\,. \qquad \alpha \simeq 1 \qquad (6.10)$$

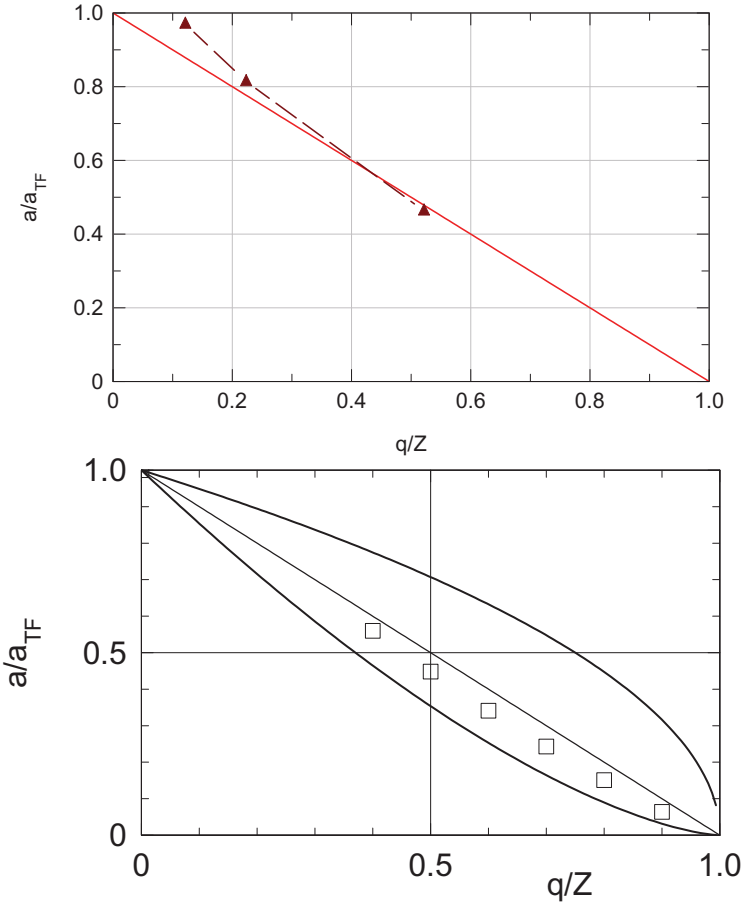

Fig. 6.2 Dependence of the Thomas-Fermi screening radius on the charge state of a positive ion. Upper graph: Comparison between (6.8) (triangles) and (6.9) (line). Lower graph: Points from Fermi and Amaldi (1934). Lines: $(1-q/Z)^{\alpha}$ with $\alpha = 0.5, 1$ and 1.5, cf. (6.10). From Sigmund (1997)

A more rigorous argument in support of (6.10), which does not make use of an exponential approximation, goes back to Fermi and Amaldi (1934). Their result is likewise shown in Fig. 6.2.

With this, Fig. 6.3 has been based on the relation

$$\frac{a_1}{a_2} = 1 - \frac{q_1}{Z_1}\,, \tag{6.11}$$

The dependence on Z_1 and Z_2 indicated in (6.3) is rather weak and has been ignored here. You may note that for a nearly-stripped ion the interaction potential depends

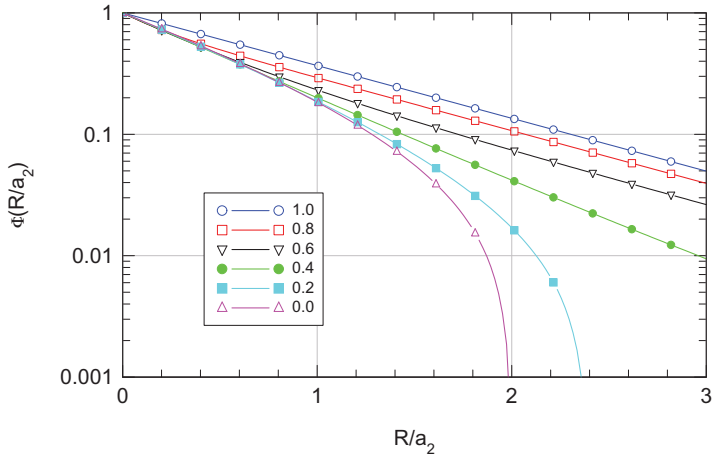

Fig. 6.3 Screening function for the interaction between a neutral atom and an ion with charge $q_1 e$ for $Z_1 = Z_2$ and $q_2 = 0$ according to (6.8)

sensitively on the charge, while such a dependence is barely visible for $R/a_2 \lesssim 0.5$ and quite small further up to $R/a_2 \sim 1.5$.

6.2.2 Thomas-Fermi Theory

Although a derivation of the interatomic potential proposed by Lindhard and Scharff was never published, an unpublished draft existed which, as far as the theoretical basis is concerned, was very similar to that underlying the theory of Firsov (1957b,a). Actually, both theories rely heavily on the work of Lenz (1932) and Jensen (1932) on the interaction between Thomas-Fermi atoms and ions as summarized by Gombas (1949).

You may recall from the discussion in Sect. 1.4 that the energy of a Thomas-Fermi atom contains a kinetic contribution, (1.15), in addition to potential (electrostatic) energy. This contribution also affects the interaction between two atoms but has been neglected in Bohr's estimate. It represents a quantum effect and takes into account that a straight overlap between stiff charge distributions may not be allowed by the Pauli principle, so that some electrons have to move up to higher (unoccupied) states.

Let us consider the energy of a diatomic molecule in the Thomas-Fermi model. An appropriate starting point is (1.18) which we may rewrite in a generalized form,

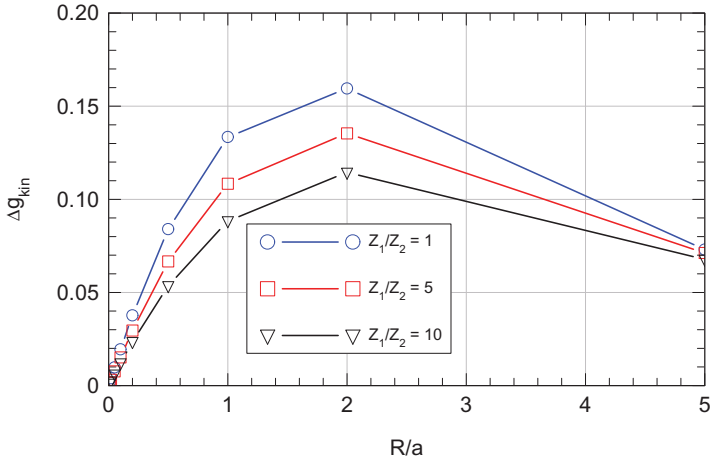

Fig. 6.4 The contribution of the kinetic-energy correction to the screening function for exponential atomic charge distributions

$$\mathcal{E} = \kappa_k \int \mathrm{d}^3\boldsymbol{r}\, \rho(\boldsymbol{r})^{5/3} - e \int \mathrm{d}^3\boldsymbol{r}\, \rho(\boldsymbol{r})\Phi_n(\boldsymbol{r}) + \frac{e^2}{2} \int \mathrm{d}^3\boldsymbol{r} \int \mathrm{d}^3\boldsymbol{r}'\, \frac{\rho(\boldsymbol{r})\rho(\boldsymbol{r}')}{|\boldsymbol{r}-\boldsymbol{r}'|} \tag{6.12}$$

for $v = 0$, where the potential $Z_1 e/r$ of the nucleus has been denoted by $\Phi_n(r)$. In this form (6.12) may also describe the electron energy of a molecule, with the replacement

$$\Phi_n(\boldsymbol{r}) = \frac{Z_1 e}{r_1} + \frac{Z_2 e}{r_2}\,. \tag{6.13}$$

You could try to determine an equilibrium configuration of the electrons in a molecule by applying the variational principle, just as has been done in case of an atom. The interaction energy between the two atoms/ions could then be found by adding the Coulomb interaction between the nuclei and subtracting the energies of the two isolated atoms. The resulting expression would represent an *adiabatic potential* in the Thomas-Fermi approximation.

Lenz (1932) and Jensen (1932) as well as Gombas (1949), aiming at this adiabatic potential, argued that a first approximation for this quantity could be found by superposition of undisturbed atomic charge distributions,

$$\rho(\boldsymbol{r}) \simeq \rho_0(\boldsymbol{r}) = \rho_1(r_1) + \rho_2(r_2)\,, \tag{6.14}$$

since the difference $\delta\rho = \rho - \rho_0$ will enter in the second order into the error in the energy.

As indicated above, with increasing relative velocity of two collision partners, straight superposition may become a more appropriate representation of the poten-

tial than adiabatic interaction. Therefore, the error made by adopting (6.14) will be even smaller in the present context.

Within this picture we may subtract the energies of the constituent atoms from (6.12) and obtain

$$\mathcal{V}(R) = \frac{Z_1 Z_2 e^2}{R} + \kappa_k \int \mathrm{d}^3\boldsymbol{r} \left[(\rho_1(r_1) + \rho_2(r_2))^{5/3} - \rho_1(r_1)^{5/3} - \rho_2(r_2)^{5/3}\right] - \int \mathrm{d}^3\boldsymbol{r} \left[\frac{Z_1 e^2}{r_1}\rho_2(r_2) + \frac{Z_2 e^2}{r_2}\rho_1(r_1)\right] + \int \mathrm{d}^3\boldsymbol{r} \int \mathrm{d}^3\boldsymbol{r}' \, \frac{e^2}{|\boldsymbol{r} - \boldsymbol{r}'|}\, \rho_1(r_1)\rho_2(r_2'). \quad (6.15)$$

for the interaction energy of two atoms. Figure 6.4 shows the contribution

$$\Delta g_{\mathrm{kin}} = \frac{R}{Z_1 Z_2 e^2} \times \kappa_k \int \mathrm{d}^3\boldsymbol{r} \left[(\rho_1(r_1) + \rho_2(r_2))^{5/3} - \rho_1(r_1)^{5/3} - \rho_2(r_2)^{5/3}\right] \quad (6.16)$$

to the screening function for a Yukawa-type charge density with Bohr's screening radius. With this choice, the result depends only on R/a and Z_1/Z_2, and the dependence on Z_1/Z_2 is not very pronounced.

Comparison of Fig. 6.4 to Fig. 5.17 indicates that the contribution of Δg_{kin} to the screened potential increases with increasing distance and eventually dominates. If you have difficulties in appreciating this, you are encouraged to look into Problem 6.3.

Equation (6.15) has served as the theoretical basis for numerous computations of interatomic potentials. Apart from computational details, theoretical schemes differ in the input, especially

- atomic charge distributions and
- possible inclusion of exchange and correlation terms.

This author is unaware of a fully analytical evaluation of the kinetic-energy contribution, (6.16). Although authors invested considerable effort in preparing the double integral for numerical evaluation, there is little reason to go into details, because straight numerical integration is no particular challenge on present-day computers.

6.2.2.1 Firsov's Estimate

The central study in the present context is the theory of Firsov (1957b,a). Note first that in quantum mechanics, an approximate solution of the Schrödinger equation leads to an overestimate of the energy of the considered system. This feature also prevails in Thomas-Fermi theory. A simple proof, following Firsov (1957b) has been

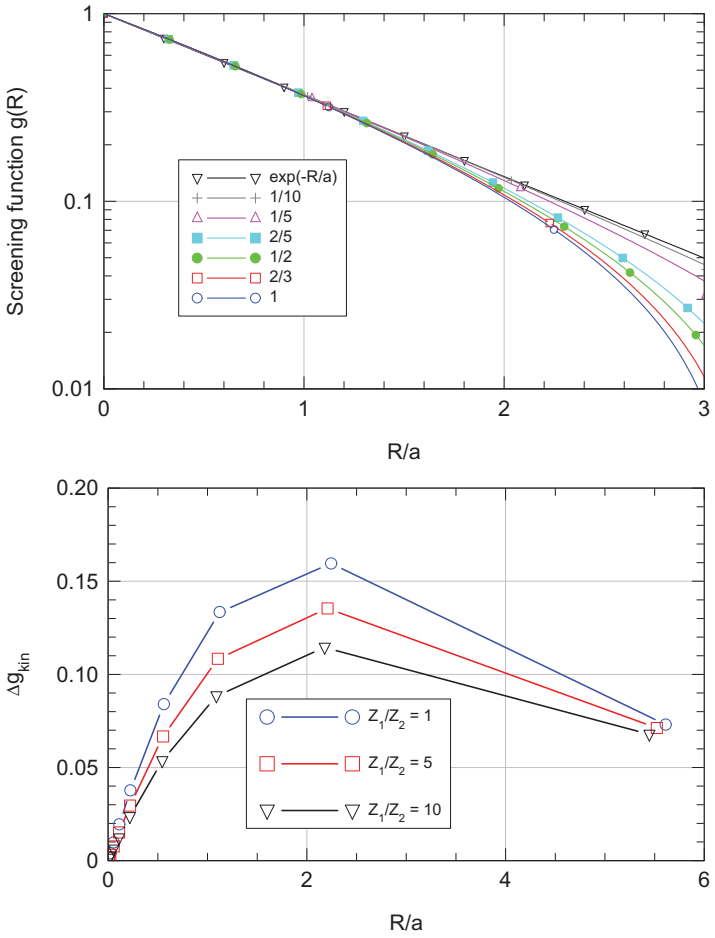

Fig. 6.5 Comparison between Bohr or Lindhard-Scharff and Firsov screening radii. Top: Figure 6.1 redrawn employing the Firsov screening radius as the abscissa variable. Bottom: Same as Fig. 6.4 for Firsov case

sketched in Problem 6.4. Superposition of atomic charge distributions is an approximation to the true charge density. Therefore, the resulting interaction potential must lead to an overestimate of the total electronic energy of the system of two atoms or ions. Firsov (1957b) also found an expression very similar to (6.15) which delivers an *upper bound* to the total energy. He also found that the difference between the two expressions, when evaluated with Thomas-Fermi input, does not exceed 5%. Note that this assumes the 'true' potential to be adiabatic.

Numerical evaluation of the two resulting potentials led Firsov (1957a) to propose

$$g(R) = g_0(R/a) \tag{6.17}$$

as an interpolation formula, where g_0 denotes the Thomas-Fermi screening function for a neutral atom and

$$a = \frac{0.8853 a_0}{\left(Z_1^{1/2} + Z_2^{1/2}\right)^{2/3}} . \tag{6.18}$$

Firsov's expression differs from Lindhard's choice only in the screening radius. You may easily convince yourself that the ratio $a_{\text{Lindhard}}/a_{\text{Firsov}}$ decreases from 1.12 to 1.04 for Z_1/Z_2 increasing from 1 to 100.

Figure 6.5 demonstrates the consequences on the scaling of the potential for Yukawa-type electron densities. The upper graph shows clearly improved scaling compared with Fig. 6.1, in particular for $R/a \lesssim 1$, where scaling is essentially perfect. On the other hand, no significant improvement of scaling is found in the kinetic contribution in comparison with Fig. 6.4.

6.2.2.2 Thomas-Fermi-Dirac Approach

Firsov's approach was extended by Abrahamson et al. (1961) to the Thomas-Fermi-Dirac scheme by including an exchange contribution in the Thomas-Fermi energy in accordance with Sect. 1.8.2. Again a maximization principle was employed in addition to the energy expression which provides a minimum. As a result of extensive numerical operations the authors suggested an interpolation formula,

$$\mathcal{V}(R) = \frac{Z_1 Z_2 e^2}{2R}\left[g_0\left(\frac{R}{a_1}\right) + g_0\left(\frac{R}{a_2}\right)\right] - \frac{\kappa_a^2}{120\kappa_k}(Z_1 + Z_2) + \bar{\Lambda}(R)\,, \tag{6.19}$$

where $a_j = 0.8853 a_0/Z_j^{1/3}$ are Thomas-Fermi radii and g_0 is the Thomas-Fermi function of a neutral atom. The last two terms in this expression, the first of which is independent of the internuclear distance R, represent the effect of the exchange term via the constant κ_a defined in (1.91).

Equation (6.19) has been applied to evaluate interaction potentials between rare-gas atoms by Abrahamson (1963b,a). The focus of those calculations was on internuclear distances far beyond the Thomas-Fermi screening radius, typically up to 6 Bohr radii, where potentials discussed here cannot be expected to provide a realistic estimate of the interaction.

Figure 6.6 shows an example for He-Ne. The potential is close to exponential for $R > a_0$, softer than Bohr's expression but harder than Thomas-Fermi screening.

As pointed out by Günther (1964), Firsov's variational principles lead to questionable results when applied to the Thomas-Fermi-Dirac model due to the finite dimensions of the atomic charge densities. Rather than abandoning the TFD model altogether, Nikulin (1971) proposed to keep the TFD functional and to insert Hartree-Fock atomic electron densities without the use of variational parameters.

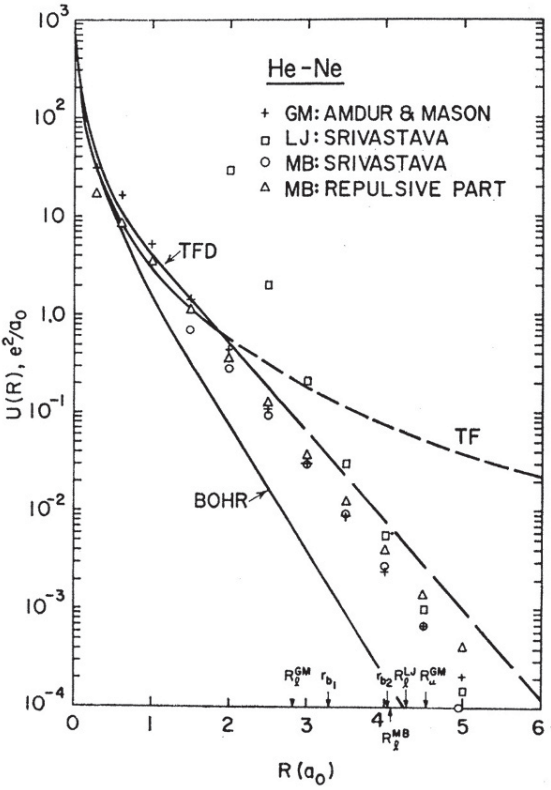

Fig. 6.6 Interaction potential between neutral He and Ne atoms according to the Thomas-Fermi-Dirac model. Also included potentials of Amdur and Mason (1956) and Srivastava (1958). From Abrahamson (1963a)

6.2.3 Other Binary Potentials

6.2.3.1 Hartree-Fock Estimates

If we accept the point of view of Firsov (1957b) that the electron density entering into the energy expression is a trial function, any physically acceptable expression for the electron density can be adopted, so that there is no reason to restrict to Thomas-Fermi-type input. Thus we can just as well apply accurate atomic electron distributions available from the literature. However, as long as interaction energies are determined by the Thomas-Fermi expression, with or without exchange-correlation, the error in such computations is substantial. In other words, subtleties in atomic wave functions will be immaterial.

The first attempt to improve the accuracy of the Thomas-Fermi model in this way were the calculations of molecular electron densities by Lenz (1932) and Jensen (1932), where a trial function, (1.59) was adopted which was not a solution of the Thomas-Fermi equation but a better approximation to reality. In the present context this idea was taken up by Wedepohl (1967) who applied electron densities calculated by Hartree and Hartree (1938) and empirical densities deduced from X-ray diffrac-

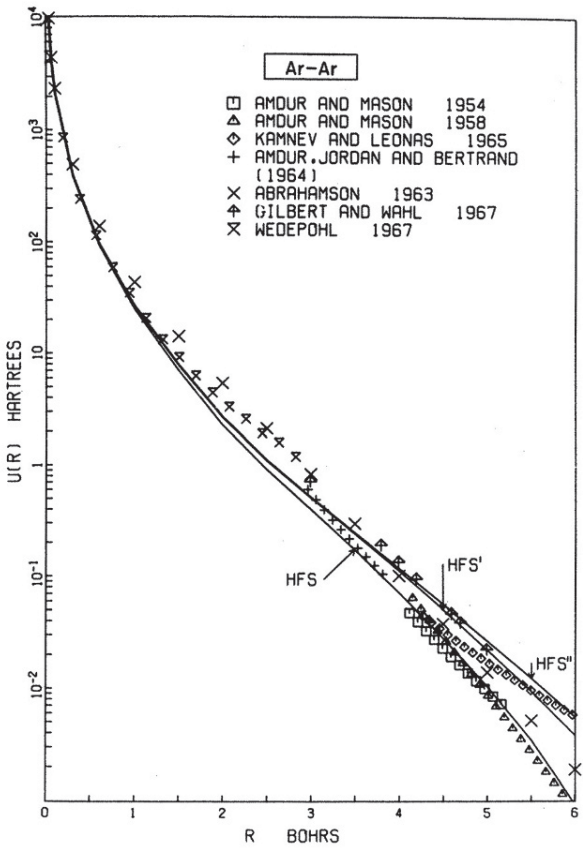

Fig. 6.7 Interaction potential between two argon atoms according to Wilson and Bisson (1971), compared with four potentials deduced from scattering measurements and three calculated potentials (Abrahamson, 1963b, Gilbert and Wahl, 1967, Wedepohl, 1967). From Wilson and Bisson (1971)

tion measurements (Witte and Wölfel, 1958). Interaction energies were calculated including the exchange term.

Wilson and Bisson (1971) applied the same scheme but used tabulations by Herman and Skillman (1963) for several homonuclear atom pairs. An example is shown in Fig. 6.7. This work was continued by Wilson et al. (1977), and results were parameterized in terms of a screening function

$$g(R) = \sum C_j \mathrm{e}^{-b_j R/a}\,, \tag{6.20}$$

which was first introduced by Molière (1947), who operated with three pairs of constants (C_j, b_j), cf. Table 6.1 and the Bohr screening radius. Results of Wilson et al. (1977) were plotted in terms of R/a_{Firsov} with $a_{\mathrm{Firsov}} = 0.8853 a_0/(Z_1^{1/2} +$

Table 6.1 Constants defining screening function (6.20) according to Molière (1947), Wilson et al. (1977) (Kr-C) and Ziegler et al. (1985) (ZBL)

Potential		Molière		Kr-C		ZBL	
C_1	b_1	0.35	0.3	0.190 945	0.278 544	0.028 17	0.201 62
C_2	b_2	0.55	1.2	0.473 674	0.637 174	0.280 22	0.402 90
C_3	b_3	0.10	6.0	0.335 381	1.919 249	0.509 86	0.942 29
C_4	b_4					0.181 75	3.199 8

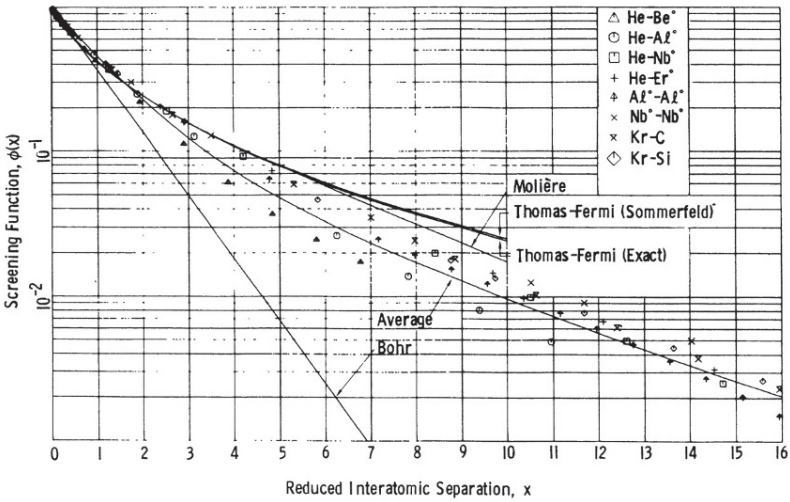

Fig. 6.8 Screening function for several atom pairs due to Wilson et al. (1977). See text. From Wilson et al. (1977)

$Z_2^{1/2})^{2/3}$, but with three pairs of constants (C_j, a_j) for each atom pair. The data set for the Kr-C pair (cf. Table 6.1) yields the so-called krypton-carbon potential, which has been frequently applied also to other atom-atom or ion-atom pairs. Examples are the data points in Fig. 6.8.

Similar computations were performed by numerous authors (Kim and Gordon, 1974, Dedkov, 1984, 1989), where also charged ions, in particular alkalis, were studied. A comprehensive review with a special emphasis on radiation physics is due to Dedkov (1995).

The work of Wilson et al. (1977) was extended to a large number of atom-atom pairs by Biersack and Ziegler (1982) and Ziegler et al. (1985), and an interpolation formula of the type of (6.20) was established with constants listed in Table 6.1 and commonly referred to as the ZBL potential.

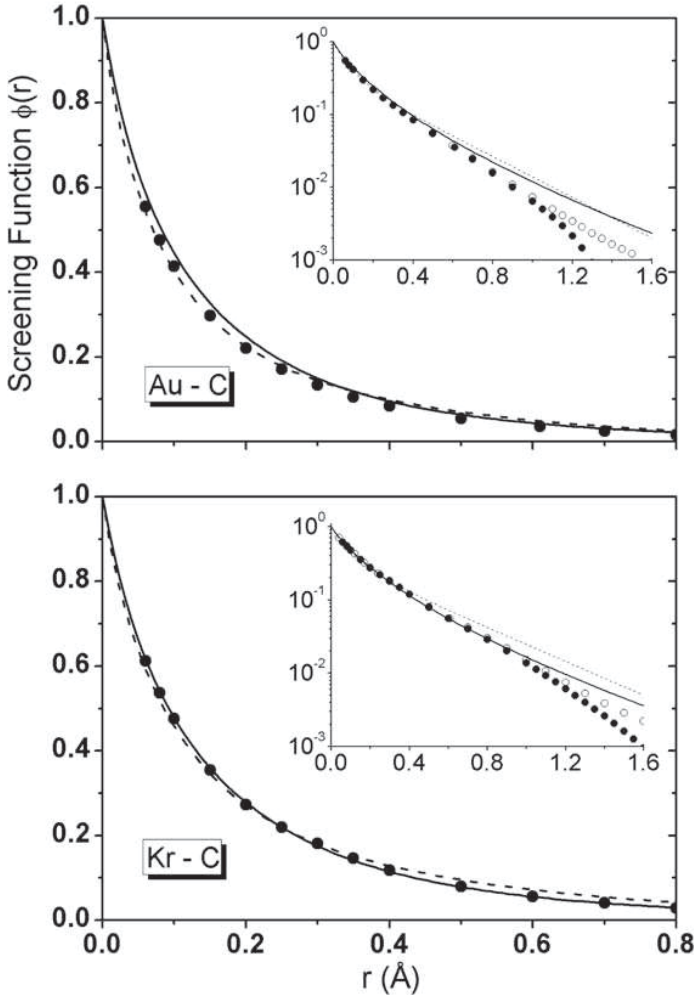

Fig. 6.9 Screening functions for Au-C and Kr-C interaction potentials. Solid circles: DFT(RESC); Empty circles: HF(RESC); solid lines: ZBL; dotted lines: Molière. From Kuzmin (2006)

6.2.3.2 Ab Initio Calculations

More recently, quantum chemistry codes have been applied to calculate interatomic potentials. The standard procedure here is to determine the ground-state energy of a molecule for a given configuration of the nuclei and to subtract the energy of the isolated atoms, i.e., one deals with *adiabatic potentials*. Apart from computational aspects the result of such calculations depends mainly on the basis set of atomic wave functions. Also relativistic effects may be taken into account.

Figure 6.9 shows two examples. Good agreement is found for $R \lesssim a_0$ between the results of two different codes, Density Functional Theory (TFD-RESC)[1] and Hartree-Fock (HF-RESC) as well as the Molière potential, whereas ZBL shows a slight difference. At larger distances substantial differences are found.

6.2.4 Nonbinary Potentials

6.2.4.1 Embedded-Medium Potentials

A useful theoretical basis for calculating interactions especially in *metals* is found in condensed-matter theory. The starting point is the problem of the electronic state of a foreign atom in a solid or at a solid surface. In the so-called effective-medium theory, the solid is replaced by a free electron gas (Nørskov, 1977, Nørskov and Lang, 1980, Stott and Zaremba, 1980, Nørskov, 1982, Daw and Baskes, 1983, 1984). The energy of such a system can be calculated by various methods, including density-functional theory. As a result one may find formation energies of point defects, chemisorption energies and the like.

Daw (1989), Adams and Foiles (1990) considered the effective interaction of two atoms embedded into an electron gas. This results in an embedded-atom potential taking proper care of the attractive part of the interaction force as well as the chemical properties of the interacting atoms.

This aspect will be discussed in some detail in connection with radiation effects in Volume 3 of this monograph.

6.2.4.2 Empirical Potentials

When simulating collision processes in solids or liquids you may need a realistic description of the equilibrium state of the medium. A convenient way to achieve such a description is to find a reasonable trial function with a number of parameters that can be fitted such as to match the known structure as well as mechanical and/or thermal properties of the material as closely as desirable. Such potentials must be attractive over a certain range of distances. An early example is the well-known Lennard-Jones or 6–12 potential (Lennard-Jones, 1924) with constants fitted to the van der Waals constants of real gases. Another empirical potential is the Born-Mayer potential, describing ionic crystals by a sum of a repulsive exponential and the Coulomb attraction between anions and cations (Born and Mayer, 1932).

More complicated structures may be described by means of many-body potentials. A useful example is the Stillinger-Weber potential characterizing silicon (Stillinger and Weber, 1985),

$$\mathcal{V} = \mathcal{V}_2 + \mathcal{V}_3 \,, \tag{6.21}$$

[1] Relativistic scheme of elimination of small components (RESC) of the four-component Dirac equation.

where $\mathcal{V}_2$ is a two-body potential with five free parameters and

$$\mathcal{V}_3(\boldsymbol{R}_i, \boldsymbol{R}_j, \boldsymbol{R}_k) = h(R_{ij}, R_{ik}, \theta_{jik}) + h(R_{ji}, R_{jk}, \theta_{ijk}) + h(R_{ki}, R_{kj}, \theta_{ikj}) \quad (6.22)$$

a three-body potential expressed by two interatomic distances and one angle, where θ_{jik} is the angle between $\boldsymbol{R}_{ji}$ and $\boldsymbol{R}_{ki}$. Expressing a three-body potential in this way facilitates the search for parameters reproducing the crystal structure.

For silicon, different sets of trial functions have become commonly used, developed by Stillinger and Weber (1985) and by Tersoff (1986). For monoatomic materials at least seven adjustable parameters enter, and a correspondingly higher number for heteroatomic substances.

Potentials describing material properties near equilibrium need to be amended such as to properly describe the behaviour at small internuclear distances. It is a requirement on the chosen parametrization that a smooth transition between the two regimes is obtainable.

6.2.5 Power Potentials

For rough estimates it is frequently useful to approximate the screening function in power form (Bohr, 1948),

$$g(\zeta) \simeq \frac{k_s}{s}\zeta^{1-s}. \quad (6.23)$$

Here the exponent s and the magnitude k_s can be determined in principle by matching (6.23) in power and slope to the actual potential. This, however, is rarely done in practice. A more efficient procedure will be mentioned in Sect. 6.4.2. Independent of the applied procedure, the exponent s depends on the range of distances where the screening function is supposed to be matched. For exponential screening, (6.5), s can take any value ≥ 1, while the Thomas-Fermi function mentioned in Sect. 6.2.2 behaves as $\propto R^{-3}$ at large distances, so the range of s-values is limited to $1 \lesssim 3$.

6.3 Screened-Coulomb Scattering

The basic tools for characterizing elastic scattering have been collected in Chap. 3, Vol. 1. The present section serves to provide specific results for ion-atom scattering under screened-Coulomb interaction.

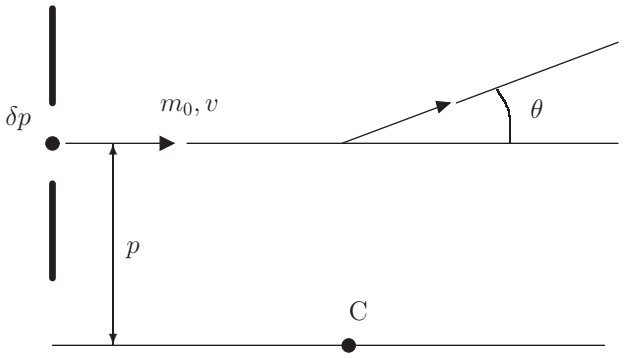

Fig. 6.10 Modified Bohr criterion for elastic scattering. See text

6.3.1 Limitations of Classical Elastic-Scattering Theory

It is a common procedure in the theory of heavy-ion penetration to treat nuclear scattering and stopping by classical scattering theory assuming elastic collisions. According to the Bohr criterion derived in Sect. 2.3.6, Vol. 1, classical scattering theory should be valid for

$$\frac{2Z_1 Z_2 e^2}{\hbar v} \gg 1 \,. \tag{6.24}$$

This defines an upper velocity limit, above which quantal scattering theory needs to be applied. That limit increases rapidly with increasing atomic numbers of the collision partners involved.

Nevertheless, some caution is indicated. Firstly, (6.24) has been derived for unscreened Coulomb interaction. An extension to screened-Coulomb interaction is evidently needed. Secondly, (6.24) assumes small-angle scattering. To what extent does it apply at large scattering angles? Thirdly, to what extent can electronic excitation and charge exchange be neglected? Let us briefly look into these aspects.

6.3.1.1 Generalization of the Bohr Criterion

A generalization of (6.24) was provided by Lindhard (1965). Figure 6.10 illustrates the scattering in the centre-of-mass frame of reference. A particle with reduced mass m_0 and velocity v passes through an aperture of width $2\delta p$ at an impact parameter p to a scattering centre C. According to the uncertainty principle, this implies a spread in transverse momentum

$$\delta P_1 \sim \frac{\hbar}{2\delta p} \,, \tag{6.25}$$

which is equivalent to a spread in scattering angle Θ,

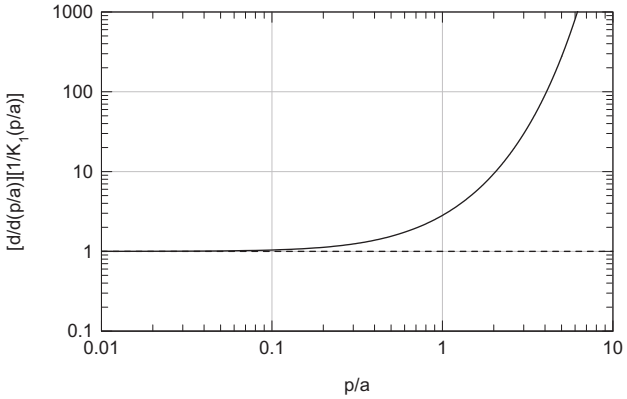

Fig. 6.11 Modified Bohr criterium. See text

$$\delta\Theta_1 \sim \frac{\delta P_1}{m_0 v}\,. \tag{6.26}$$

Conversely, the spread in impact parameter δp leads to a spread in scattering angle

$$\delta\Theta_2 = \left|\frac{\mathrm{d}\Theta}{\mathrm{d}p}\right| \delta p\,. \tag{6.27}$$

The total spread is then found as

$$\delta\Theta^2 = \delta\Theta_1^2 + \delta\Theta_2^2\,. \tag{6.28}$$

This quantity has a minimum at

$$\delta p^2 = \frac{\hbar}{2m_0 v|d\Theta/dp|}\,, \tag{6.29}$$

where

$$\delta\Theta^2_{\min} = \frac{\hbar|\mathrm{d}\Theta/\mathrm{d}p|}{m_0 v}\,. \tag{6.30}$$

According to Bohr (1948), a classical description is approximately valid if the spread in scattering angle $\delta\Theta$ is small compared to the scattering angle Θ itself. The resulting criterion can be written in the form

$$\left|\frac{\mathrm{d}}{\mathrm{d}p}\frac{1}{\Theta(p)}\right| \ll \frac{m_0 v}{\hbar}\,. \tag{6.31}$$

You can easily convince yourself that this reduces to (6.24) for Coulomb interaction. However, the fact that the scattering angle occurs in the denominator in (6.31) indicates a modification in particular at small angles.

As an example, consider two particles interacting via the Bohr potential

$$\mathcal{V}(R) = \frac{Z_1 Z_2 e^2}{R} \mathrm{e}^{-R/a} , \tag{6.32}$$

cf. (6.7). In problem 6.5 you will find that, for large impact parameters or small angles, (6.31) reduces to

$$\kappa \equiv \frac{2Z_1 Z_2 e^2}{\hbar v} \gg \left| \frac{\mathrm{d}}{\mathrm{d}(p/a)} \frac{1}{K_1(p/a)} \right| , \tag{6.33}$$

where $K_1(z)$ is a modified Bessel function in standard notation (Abramowitz and Stegun, 1964).

The function on the right-hand side of (6.33) has been drawn up in Fig. 6.11. You may note that the quantity on the left side of (6.33) is Bohr's kappa as introduced in (2.80), Vol. 1. For Coulomb interaction that quantity needs to exceed 1, the stipled line in Fig. 6.11. For screened interaction no change occurs at small impact parameters, $p \ll a$, where the potential is Coulomb-like (cf. the stipled line), while the solid line, valid for the Bohr potential, rises steeply from $p/a \sim 1$ on, thus making it increasingly difficult to fulfill the modified Bohr criterion. However, for heavy collision partners and $v \ll v_0$, a situation typical for applications in radiation damage, ion implantation etc, κ is much greater than 1. Therefore it makes sense to extend the ordinate scale in Fig. 6.11 to the level indicated in the graph.

6.3.1.2 Quantal Effects

The assumption of small-angle scattering is not critical to the derivation of the modified Bohr criterion presented in the previous section. Moreover, Fig. 6.11 does not give rise to concern about larger scattering angles (or smaller impact parameters). An exception is straight backscattering at 180°, where one might be concerned about interference between the incoming and outgoing wave (Sect. 7.8.3).

Quantal effects are, however, observable in the scattering of heavy particles. One of the most drastic ones is charge exchange, discussed in Chap. 2. Charge exchange may show pronounced variations with beam energy and scattering angle (Ziemba and Everhart, 1959, Lockwood et al., 1963). This implies that dependent on the detection device, measured distributions in angle or energy may deviate dramatically from the smooth spectra expected from classical scattering theory.

Inelastic energy loss by electron excitation or ionization affects conservation laws and thus angular as well as energy distributions of scattered particles. In fact, inelastic energy losses can be determined experimentally in this way, as was discussed in Problems 3.4 and 3.5, Vol. 1.

6.3.2 Recapitulation

6.3.2.1 Classical Scattering Integral

The central result of classical binary scattering theory is contained in (3.34) and (3.35), Vol. 1, which relates the scattering angle Θ in the centre-of-mass frame to the impact parameter p by

$$\Theta = \pi - 2p \int_{R_m}^{\infty} \frac{\mathrm{d}R}{R^2} \left(1 - \frac{\mathcal{V}(R)}{E_r} - \frac{p^2}{R^2}\right)^{-1/2} , \tag{6.34}$$

where $E_r = m_0 v^2/2$ is the relative kinetic energy and R_m the closest distance of approach that satisfies the relation

$$1 - \frac{\mathcal{V}(R_m)}{E_r} - \frac{p^2}{R_m^2} = 0 . \tag{6.35}$$

For screened-Coulomb interaction (6.4) or

$$\mathcal{V}(R) = \frac{Z_1 Z_2 e^2}{R} g(R/a) , \tag{6.36}$$

(6.34) reduces to

$$\Theta = \pi - 2p \int_{R_m}^{\infty} \frac{\mathrm{d}R}{R^2} \left[1 - \frac{a}{\epsilon R} g\left(\frac{R}{a}\right) - \frac{p^2}{R^2}\right]^{-1/2} \tag{6.37}$$

with

$$\epsilon = \frac{a E_r}{Z_1 Z_2 e^2} \tag{6.38}$$

in accordance with (3.50), Vol. 1. Introducing a dimensionless impact parameter

$$\xi = \frac{p}{a} \tag{6.39}$$

you find

$$\Theta = \pi - 2\xi \int_{\zeta_m}^{\infty} \frac{\mathrm{d}\zeta}{\zeta^2} \left(1 - \frac{g(\zeta)}{\epsilon\zeta} - \frac{\xi^2}{\zeta^2}\right)^{-1/2} , \tag{6.40}$$

where $\zeta_m = R_m/a$.

6.3.2.2 Scaling Properties

Equation (6.40) expresses the scattering angle as a function of ϵ and ξ,

$$\Theta = \Theta(\epsilon, p/a) . \tag{6.41}$$

You may write this relation in the form

$$p = ah\left(\epsilon, \sin\frac{\Theta}{2}\right), \tag{6.42}$$

and thus

$$\mathrm{d}\sigma = \left|\pi \mathrm{d}p^2\right| = \pi a^2 g_1\left(\epsilon, \sin^2\frac{\Theta}{2}\right)\mathrm{d}\sin^2\frac{\Theta}{2}, \tag{6.43}$$

where h and g_1 are functions determined by the screening function g.

The relation to the energy transfer is given by (3.8), Vol. 1,

$$T = \gamma E \sin^2\frac{\Theta}{2} \tag{6.44}$$

with

$$\gamma = \frac{4M_1M_2}{(M_1+M_2)^2} \tag{6.45}$$

for nonrelativistic collisions.

6.3.2.3 Classical Small-Angle Scattering

In Chap. 3.3.6, Vol. 1, an expansion of the classical scattering integral, (6.40) in powers of the interaction was found. The first term in this expansion, called momentum approximation, reads

$$\Theta = -\frac{1}{pE_r}\int_p^\infty \frac{\mathrm{d}r}{\sqrt{1-p^2/r^2}}\frac{\mathrm{d}}{\mathrm{d}r}\left[r\mathcal{V}(r)\right] \tag{6.46}$$

or, for screened-Coulomb interaction,

$$\Theta = -\frac{1}{\epsilon p/a}\int_{p/a}^\infty \frac{\mathrm{d}\zeta}{\sqrt{1-(p/a)^2/\zeta^2}}\frac{\mathrm{d}g(\zeta)}{\mathrm{d}\zeta}. \tag{6.47}$$

Equation (6.47) must be expected to accurately characterize the scattering law at sufficiently small angles.

6.3.3 Lindhard-Scharff Scaling

In addition to (6.43), which is an exact scaling property for classical elastic scattering on a screened Coulomb potential, Lindhard et al. (1968) derived an approximate scaling relationship which reduces the function $g(\epsilon, \sin^2\Theta/2)$ to a function of just one variable.

6.3.3.1 Power Potential

Following their argument, consider first the case of a power potential, where

$$g\left(\frac{R}{a}\right) = \frac{k_s}{s}\left(\frac{a}{R}\right)^{s-1}, \tag{6.48}$$

where $s > 1$ and k_s a constant. With this, (6.47) reduces to

$$\Theta = \frac{(s-1)k_s}{s\epsilon(p/a)^s}\int_1^\infty \mathrm{d}t\,\frac{t^{1-s}}{\sqrt{t^2-1}}\,. \tag{6.49}$$

The integral may be reduced to a standard form by substituting $t = 1/\sin u$. With this you find

$$\Theta = \frac{k_s\gamma_s}{\epsilon}\left(\frac{a}{p}\right)^s, \tag{6.50}$$

where

$$\gamma_s = \frac{1}{2}B\left(\frac{1}{2}, \frac{s+1}{2}\right) \tag{6.51}$$

and $B(x, y)$ is the beta function

$$B(x, y) = \int_0^1 \mathrm{d}t\,t^{x-1}(1-t)^{y-1} = \frac{\Gamma(x)\Gamma(y)}{\Gamma(x+y)}\,. \tag{6.52}$$

in the conventional definition (Abramowitz and Stegun, 1964).

6.3.3.2 Extrapolation

Equation (6.50) has a divergence at $p = 0$ instead of the expected result $\Theta = \pi$. In order to correct for this, Lindhard et al. (1968) made a bold wide-angle approximation by replacing

$$\Theta \to 2\sin\Theta/2 \tag{6.53}$$

$$p \to \sqrt{p^2 + p_0^2} \tag{6.54}$$

with a quantity p_0 to be determined by the requirement that $\Theta = \pi$ for $p = 0$, so that

$$2\epsilon = \frac{k_s}{2}B(1/2, (s+1)/2)(a/p_0)^s\,. \tag{6.55}$$

The substitution (6.54) has the convenience that p_0 drops out in the differential cross section with Θ as a variable, since

$$2\pi p\mathrm{d}p \equiv \pi\mathrm{d}p^2 \equiv \pi\mathrm{d}(p^2 + p_0^2)\,. \tag{6.56}$$

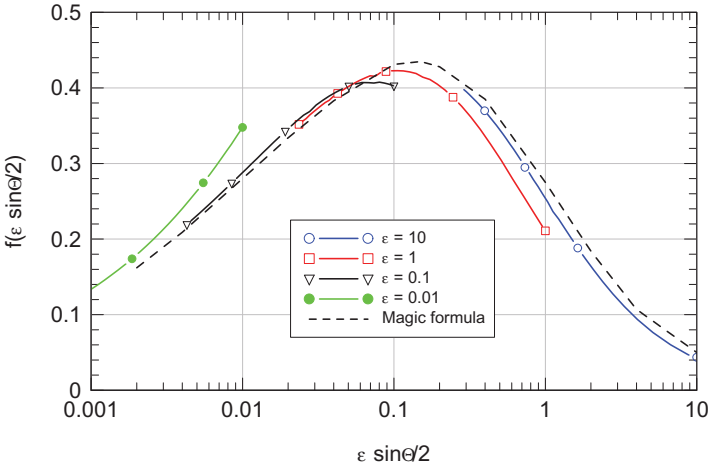

Fig. 6.12 Differential cross section for the Thomas-Fermi potential plotted in Lindhard-Scharff units. See text

With this, one may expect that the function $g(\epsilon, \sin\Theta/2)$ is approximately a function of the product $\epsilon \sin\Theta/2$, which approaches $\epsilon\Theta/2$ implied by (6.50) in the small-angle limit.

6.3.3.3 Verification

The standard form of the Lindhard-Scharff scaling relation reads as

$$\mathrm{d}\sigma(\Theta) = \pi a^2 \frac{\mathrm{d}\left(\epsilon \sin\frac{\Theta}{2}\right)}{\epsilon^2 \sin^2\frac{\Theta}{2}} f\left(\epsilon \sin\frac{\Theta}{2}\right) \tag{6.57}$$

with a yet unknown function $f(\epsilon \sin\Theta/2)$.

Scattering angles for the Sommerfeld approximation of the Thomas-Fermi potential have been evaluated numerically and tabulated by Robinson (1970). These cross sections have been plotted in Fig. 6.12 for ϵ ranging from 0.01 to 10. It is seen that Lindhard-Scharff scaling is fulfilled within a 10–20% error margin. A similar result was found for the Bohr potential in the original paper (Lindhard et al., 1968).

6.3.3.4 Magic Formula

While exact evaluation of scattering integrals is no longer a challenge, an accurate analytical approximation is still attractive. A ‘magic formula’ found by Lindhard et al. (1968) takes its starting point at the power law (6.50).

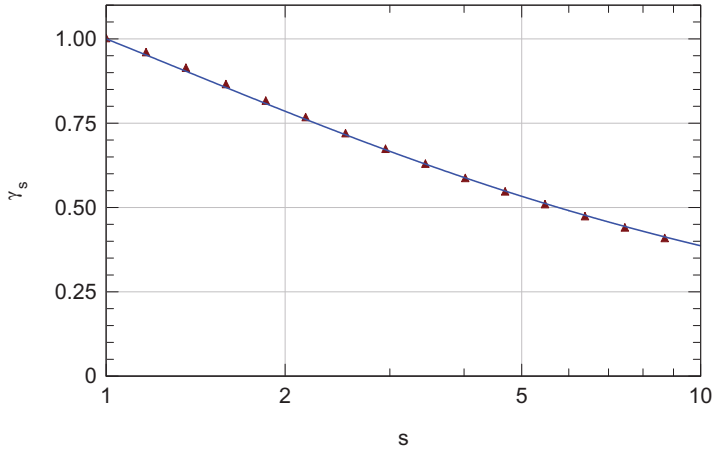

Fig. 6.13 The function γ_s, (6.51) (solid line) compared with the approximation γ'_s, (6.58) (points)

Figure 6.13 shows that the function γ_s is accurately approximated by the expression

$$\gamma'_s = \frac{1}{s}\sqrt{\frac{3s-1}{2}}\,. \tag{6.58}$$

Inserting γ'_s for γ_s and noting that the function $1/sp^s$ is proportional to the potential, you may write (6.50) in the form

$$\Theta^2 = -\frac{3}{4}p^3\frac{\mathrm{d}}{\mathrm{d}p}\left(p^{2/3}V(p)^2\right)\,. \tag{6.59}$$

This may be extrapolated to large angles in the way sketched in Sect. 6.3.3.2, but as mentioned there, this extrapolation does not affect the differential cross section.

The result of applying the magic formula to the Thomas-Fermi potential has been included in Fig. 6.12.

6.3.4 Comparison of Differential Cross Sections

The function $f(\eta)$ with

$$\eta = \epsilon \sin\frac{\Theta}{2} \tag{6.60}$$

is a convenient tool to compare differential cross sections originating in different scattering potentials. A convenient parametrization of $f(\eta)$ was found by Winterbon et al. (1970),

$$f(\eta) \simeq \frac{\lambda\eta^{1-2m}}{\left(1+\left[2\lambda\eta^{2(1-m)}\right]^q\right)^{1/q}}\,, \tag{6.61}$$

Table 6.2 Coefficients entering scaling function $f(\eta)$ for differential scattering cross section, (6.61) according to Winterbon (1972)

Screening function u	m	q	λ
Thomas-Fermi	0.333	0.667	1.309
Thomas-Fermi-Sommerfeld	0.311	0.588	1.70
Lenz-Jensen	0.191	0.512	2.92
Molière	0.216	0.570	2.37
Bohr	0.103	0.570	2.37

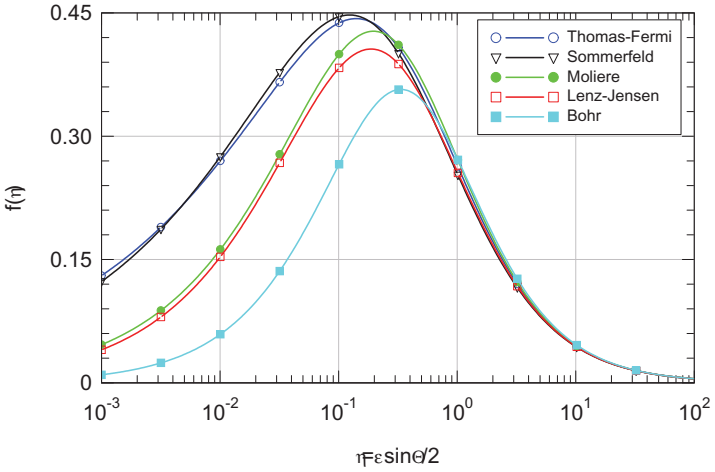

Fig. 6.14 Reduced differential cross section for several screened-Coulomb potentials, (6.61) with coefficients from Table 6.2

and parameters for several screening functions may be found in Table 6.2.

6.3.5 Inversion

Equation (6.34) expresses the scattering angle by the impact parameter and the beam energy, if the potential is given as a function of distance. You may ask whether that relation can be inverted, such that the potential can be determined from scattering measurements.

This type of inversion problem occurs in many fields of science. In the present context, relevant information can be found by varying the beam energy at a fixed scattering angle or vice versa, or a combination of the two. A scheme operating at a fixed scattering angle was proposed by Hoyt (1939), based on the solution of a related problem by Klein (1932). For the case of fixed beam energy and variable angle a similar scheme has been developed by Firsov (1953) and applied successfully in the analysis of experimental data.

In deriving Firsov's formula I am following Lane and Everhart (1960). Starting at (6.34) we may introduce a function

$$\Psi(R) = R^2 \left(1 - \frac{\mathcal{V}(R)}{E_r}\right), \tag{6.62}$$

so that

$$\Theta(p) = \pi - 2p \int_{R_m}^{\infty} \frac{\mathrm{d}R}{R} \frac{1}{\sqrt{\Psi(R) - p^2}} \tag{6.63}$$

Replacement of R by Ψ as the integration variable leads to

$$\Theta(p) = \pi - 2p \int_{p^2}^{\infty} \frac{\mathrm{d}\Psi}{\sqrt{\Psi - p^2}} \frac{\mathrm{d}(\ln R(\Psi))}{\mathrm{d}\Psi}, \tag{6.64}$$

since $\Psi(R_m) = p^2$, as follows from (6.34).

Now, the constant π can be expressed as

$$\pi = p \int_{p^2}^{\infty} \frac{\mathrm{d}\Psi}{\sqrt{\Psi - p^2}} \frac{\mathrm{d}\ln\Psi}{\mathrm{d}\Psi}, \tag{6.65}$$

as you may verify by carrying out the integration on the right-hand side. With this we arrive at

$$\Theta(p) = p \int_{p^2}^{\infty} \frac{\mathrm{d}\Psi'}{\sqrt{\Psi' - p^2}} \frac{\mathrm{d}}{\mathrm{d}\Psi'} \ln\left(\frac{\Psi'}{R(\Psi')^2}\right), \tag{6.66}$$

where the integration variable has been renamed to Ψ'.

After multiplying this equation by $1/\sqrt{p^2 - \Psi}$ and integrating from $p = \sqrt{\Psi}$ to infinity, and interchanging the order of integrations you find

$$\int_{\sqrt{\Psi}}^{\infty} \mathrm{d}p \frac{\Theta(p)}{\sqrt{p^2 - \Psi}} = \frac{1}{2} \int_{\Psi}^{\infty} \mathrm{d}\Psi' \frac{\mathrm{d}}{\mathrm{d}\Psi'} \left(\ln \frac{\Psi'}{R(\Psi')^2}\right) \int_{\Psi}^{\Psi'} \frac{\mathrm{d}p^2}{\sqrt{(\Psi' - p^2)(p^2 - \Psi)}}. \tag{6.67}$$

Since the integral over $\mathrm{d}p^2$ reduces to π, we arrive at

$$\int_{\sqrt{\Psi}}^{\infty} \mathrm{d}p \frac{\Theta(p)}{\sqrt{p^2 - \Psi}} = \frac{\pi}{2} \left(\ln \frac{\Psi'}{R(\Psi')^2}\right)_{\Psi'=\Psi}^{\infty} \equiv \frac{\pi}{2} \left(\ln \frac{\Psi(R')}{R'^2}\right)_{R'=R}^{\infty} \tag{6.68}$$

or

$$\int_{\sqrt{\Psi}}^{\infty} \mathrm{d}p \frac{\Theta(p)}{\sqrt{p^2 - \Psi}} = \frac{\pi}{2} \ln\left(\frac{R^2}{\Psi}\right). \tag{6.69}$$

Note that $\Psi(R)/R^2$ approaches 1 for large R according to the definition.

Equation (6.69) expresses R as a function of Ψ and, hence, of V/E_r. You may verify its validity on the example discussed in Problem 6.7.

Lane and Everhart (1960) have demonstrated that an interaction potential actually can be extracted by inversion of scattering data. However, the procedure is by no means trivial in practice. The first step is to express a measured differential cross section in centre-of-mass coordinates. The second step is an integration according to

$$\int_{\Theta'=\Theta}^{\pi} \mathrm{d}\sigma(\Theta') = \int_0^p 2\pi p' \mathrm{d}p' \,. \tag{6.70}$$

Typically the coverage with data points in the interval $0 \leq \Theta \leq \pi$ is incomplete. As a minimum, this limits the range of distances or energies covered by the deduced potential. Next, in order to allow integration as required in (6.69), some inter- or extrapolation may have to made, and finally, the potential has to be extracted from an implicit connection between Ψ and R.

The uniqueness of the inversion process has likewise been studied. Note first that Rutherford's cross section is identical for attractive and repulsive Coulomb interaction. Apart from that, a study by Demkov et al. (1971) indicates that the procedure becomes nonunique in case of cut-off potentials.

Figure 6.15 shows an example of a successful inversion. Lane and Everhart (1960) measured angular distributions of Ar^+ ions on Ar from about 1° to 40°. The top graph shows the data for 25 keV. The bottom graph shows potentials extracted from cross sections measured at 25, 50, and 100 keV (solid lines), as well as the Firsov (dotted) and Bohr (dashed) potentials. The near-coincidence of the three extracted potentials provides confidence both in the data and the procedure. Evidently, increasing the beam energy allows determination of the potential at smaller internuclear distances.

Potentials extracted from collision experiments are needed mostly for application in collision studies. Therefore, it appears more appropriate to compare measured to calculated cross sections, rather than comparing potentials found by inversion to calculated potentials.

6.3.6 Scattering Experiments

Direct measurements of differential cross sections are done on isolated target atoms. Data exist mainly for noble-gas targets. Early systematic measurements were performed by Everhart and coworkers, starting with Everhart et al. (1955), including the study of Lane and Everhart (1960) quoted above. The focus in this program, as well as in a parallel study by Fedorenko and coworkers (Kaminker and Fedorenko, 1955) changed gradually into inelastic processes.

Only few studies have been performed subsequently of ion-atom scattering aiming at interatomic potentials in the repulsive (keV) regime. Here I like to mention a couple of examples.

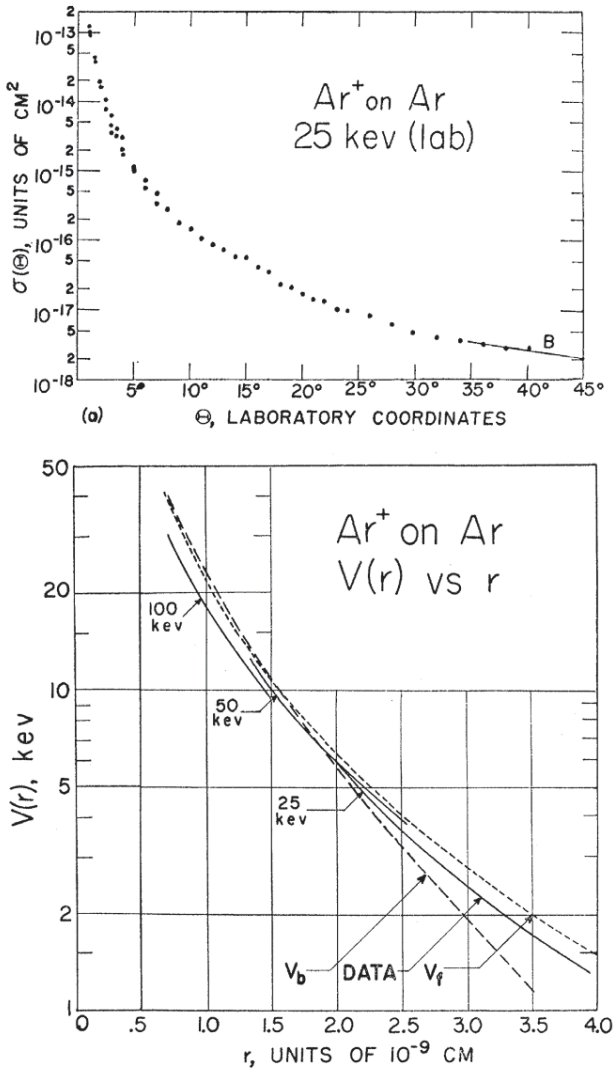

Fig. 6.15 Inversion of Ar^+-Ar differential scattering cross section (top) and the resulting potential (bottom). See text. From Lane and Everhart (1960)

6.3.6.1 Oscillatory Structure

Figures 6.16 and 6.17 show cross sections measured on xenon gas by Loftager et al. (1979). The abscissa variable is $\eta = \epsilon \sin \Theta$, and plotted is the ratio between the measured cross section in centre-of-mass variables and the Lenz-Jensen cross section. In Fig. 6.16, showing Ar on Xe, data referring to beam energies from 2.5 to

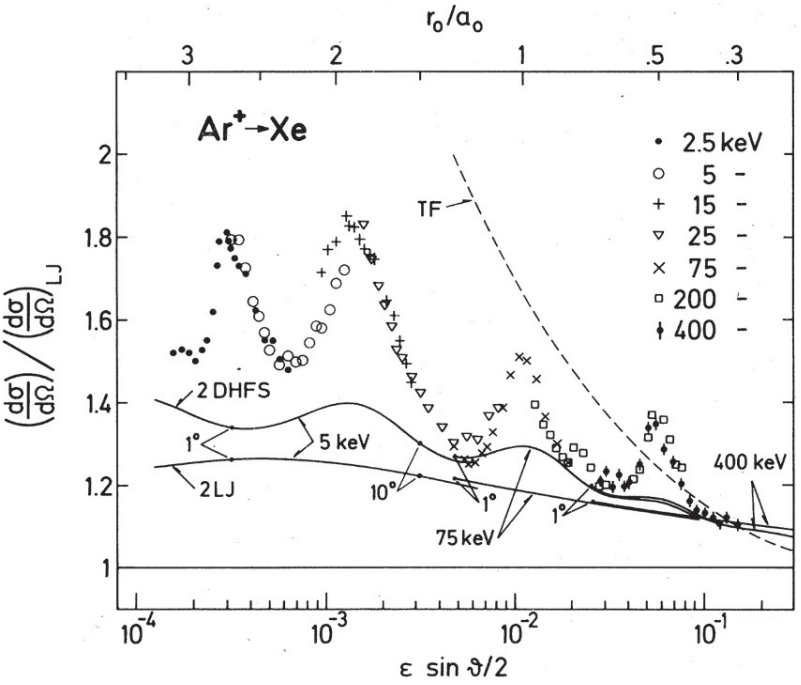

Fig. 6.16 Measured differential cross sections of Ar^+ on xenon. Plotted is the ratio between measurement and the Lenz-Jensen cross section (Lindhard et al., 1968) with the adopted screening radius $a = 0.8853a_0/\sqrt{Z_1^{2/3} + Z_2^{2/3}}$. Abscissa reduced to Lindhard variable $\eta = \epsilon \sin\Theta/2$. Also included: TF (Thomas-Fermi) (Lindhard et al., 1968). r_0 represents the closest distance of approach calculated for interaction potential based on superimposed LJ (2LJ) or Hartree-Fock (2DHFS) atomic charge densities. From Loftager et al. (1979)

400 keV fall essentially on one line, in agreement with the scaling relation (6.57). Loftager et al. (1979) concluded from this that scattering has been elastic.

Figure 6.17 shows data for C, Ne, Kr, Xe and Cd ions on Xe. You may first notice that with the exception of a small part of the C-Xe data, all experimental points fall in between the Thomas-Fermi and the Lenz-Jensen curve. Moreover, within a 20% margin, Lindhard-Scharff scaling is well obeyed for $\epsilon \sin\Theta/2 \gtrsim 0.002$, while major differences between different ions are found in the opposite end.

All data shown in Figs. 6.16 and 6.17 show an oscillatory structure which was found earlier (Loftager and Hermann, 1968, Afrosimov et al., 1972) and which has been ascribed to shell effects by Afrosimov et al. (1972). There are several possible reasons for such oscillatory structures. Very pronounced effects are found if scattered particles are recorded separately according to charge states (Ziemba and Everhart, 1959, Aberth et al., 1965). Loftager et al. (1979) found that differential cross sections for an interatomic potential allowing for shell structure (labelled DHFS in Fig. 6.17) show weak oscillations with a phase in good agreement with experiment.

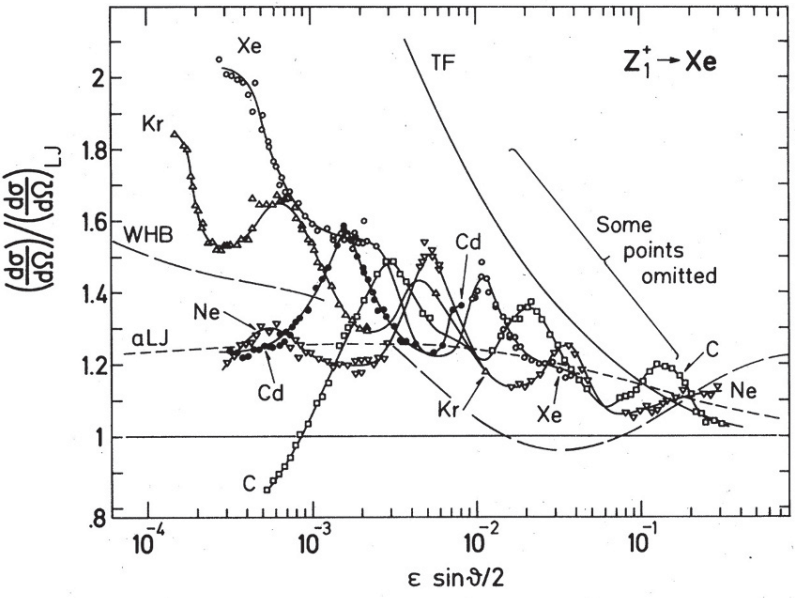

Fig. 6.17 Same as Fig. 6.16 for different ions on xenon. Also included: TF (Thomas-Fermi) (Lindhard et al., 1968), WHB (Wilson et al., 1977), aLJ (suggested average). From Loftager et al. (1979)

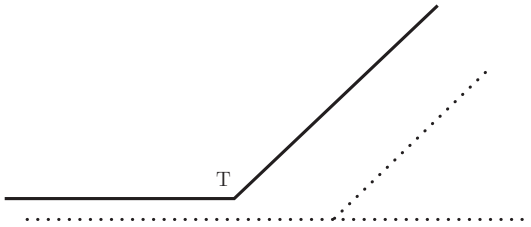

Fig. 6.18 Angular deflection in inelastic scattering. Schematic and exaggerated. See text

An explanation of the observations in Figs. 6.16 and 6.17 in terms of inelasticity (Afrosimov et al., 1972) appears most plausible: In Fig. 6.18 you find the sketch of an inelastic scattering event in the centre-of-mass frame. The only difference to the standard case of scattering on a central-force potential is an inelastic energy loss which, for simplicity, is assumed to take place at the apsis T. When arriving at T the particle has a certain angular momentum around the force centre which must be conserved. Since speed is reduced, the deflection angle and the impact parameter will increase. A quantitative discussion was given by Hartung et al. (1985) with near-perfect agreement between experiment and theory.

An experimental and theoretical study of pertinent processes and their respective contributions to the differential cross section, involving doubly-differential distributions in angle and energy as well as separation of charge states, has been performed on Na^+-Ne by Olsen et al. (1979). Figure 6.19 indicates that the contribution of

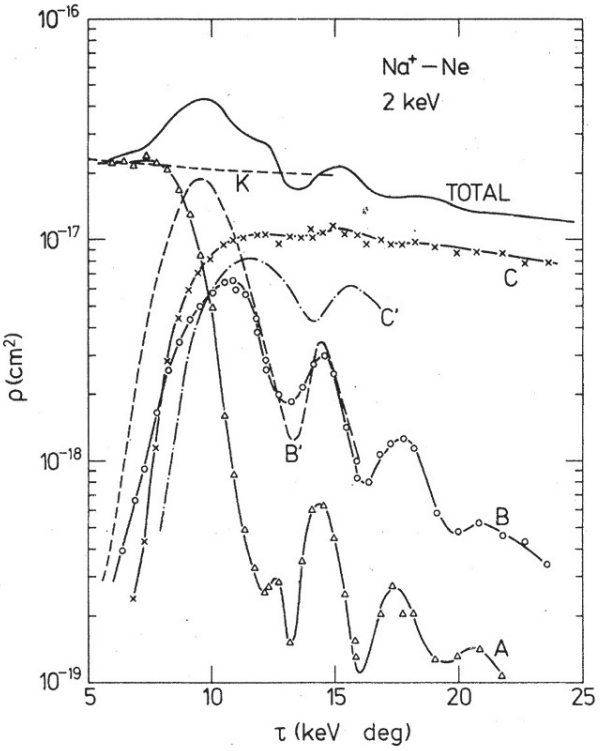

Fig. 6.19 Differential cross sections for 2 keV Na^+-Ne according to Olsen et al. (1979). A: Elastic; B: One-electron processes; C: Two-electron processes. K: Elastic scattering ignoring all electronic processes. From Olsen et al. (1979)

truly elastic collisions to the differential cross section (label A) may be very small—$\sim 1\%$ in this case—while ignoring all inelasticity (label K) may well lead to a result of the right order of magnitude (label TOTAL).

6.3.6.2 Inversion

An extensive effort to extract interatomic potentials from differential cross sections has been made by Zinoviev (2011). Literature data for a number of ion-target combinations were analyzed by the Firsov procedure described in Sect. 6.3.5. Figure 6.20 shows results plotted as a function of R/a_f, where a_f is a screening radius defined as

$$a_f = \frac{0.8853 a_0}{(Z_1^\alpha + Z_2^\alpha)^\beta} \tag{6.71}$$

with $\alpha = 1/2$ and $\beta = 2/3$.

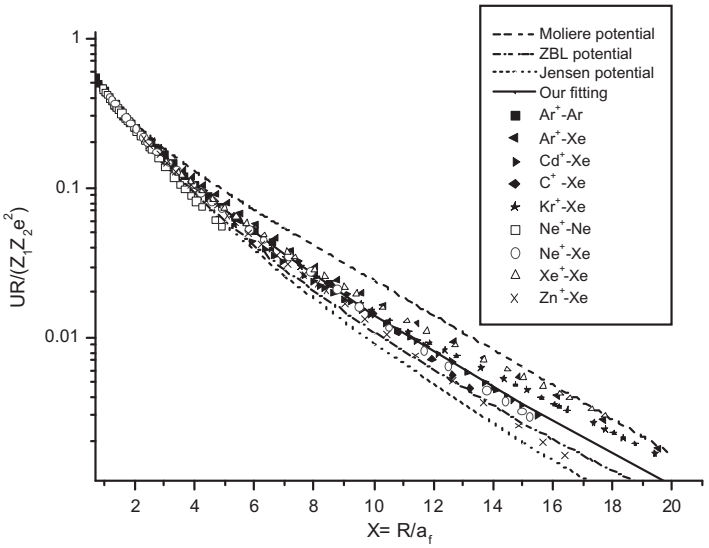

Fig. 6.20 Screening function $g(R/a)$ extracted from experimental scattering data by Firsov inversion. a_f denotes the Firsov screening radius. From Zinoviev (2011)

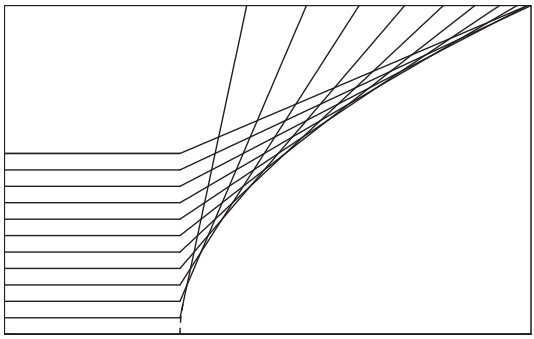

Fig. 6.21 Shadow cone in small-angle Rutherford scattering. See text

6.3.7 Shadow Cone

Imagine a homogeneous beam of particles scattered on a hard sphere of radius a with a mass much greater than the mass of a single projectile. Then, particles hitting the sphere will be scattered out of the beam. As a result there will be a cylindrical region behind the sphere where no moving particles will be detected. In other words, the sphere generates a cylindrical shadow of radius a.

What form of shadow can we expect when scattering obeys Rutherford's law rather than billiard-ball dynamics? This question was asked by Lindhard (1965), who provided an answer involving small-angle scattering.

Following Lindhard's argument, note first that for small scattering angles, (3.42), Vol. 1, reduces to

$$\Theta = \frac{b}{p}; \qquad b = \frac{2Z_1 Z_2 e^2}{M_0 v^2} \tag{6.72}$$

or, in the laboratory frame of reference,

$$\phi = \frac{Z_1 Z_2 e^2}{Ep}\,, \tag{6.73}$$

where ϕ is the scattering angle of the projectile, E the beam energy and p the impact parameter. Still assuming small angles we may place a coordinate system (x, y) in the impact plane, so that a single trajectory may be approximated by two straight lines

$$y = \begin{cases} p & \text{for } x < 0 \\ p + (Z_1 Z_2 e^2/Ep)x & \text{for } x > 0 \end{cases} \tag{6.74}$$

Such trajectories have been plotted in Fig. 6.21. Instead of a plain cylinder, we now find a parabolic cylinder which follows the relation

$$y = 2\sqrt{\frac{Z_1 Z_2 e^2}{E}x}\,. \tag{6.75}$$

Target particles lying within this 'shadow cone' will not be hit by the beam, regardless of the impact parameter. Specifically, if you want to hit a target particle at some distance $x = d$ behind the first target atom, you have to tilt the beam by an angle

$$\Delta\phi > \Theta_c = \frac{y(d)}{d} = 2\sqrt{\frac{Z_1 Z_2 e^2}{Ed}}\,. \tag{6.76}$$

This is a useful relation in the study of channeling, cf. Sect. i.1.1, Vol. 1. We shall come back to this in Appendix 11.

The shadow cone has come to play an important role in ion-surface scattering at energies well below the Rutherford regime. Accurate calculations (Oen, 1983) may have to avoid the small-angle approximation and may need to take into account the time integral, cf. Sect. 3.3.4, Vol. 1. Alternatively, trajectories may be simulated (Yamamura and Takeuchi, 1984).

6.4 Nuclear Stopping

According to Sects. 2.2.3-.2.2.5, Vol. 1, the energy loss in an elastic binary collision may be characterized by the nuclear stopping force

$$\left(-\frac{\mathrm{d}E}{\mathrm{d}x}\right)_n = NS_n \tag{6.77}$$

with

$$S_n = \int T_n \, \mathrm{d}\sigma \tag{6.78}$$

and

$$T_n = \gamma E \sin^2 \frac{\Theta}{2} \,, \tag{6.79}$$

where $\gamma = 4M_1M_2/(M_1 + M_2)^2$.

If you have a tabulation of the scattering integral (6.34) for a given potential, the nuclear stopping cross section S_n can be found by integration,

$$S_n = \gamma E \int_0^\infty 2\pi p \, \mathrm{d}p \, \sin^2 \frac{\Theta(p)}{2} \tag{6.80}$$

without going over the differential cross section.

6.4.1 Scaling Properties

Conversely, making use of the scaling relations for the differential cross section in Sect. 6.3.2.2 you find

$$\left(-\frac{\mathrm{d}E}{\mathrm{d}x}\right)_n = N\pi a^2 \gamma E \int_0^\pi g\left(\epsilon, \sin^2 \frac{\Theta}{2}\right) \mathrm{d} \sin^2 \frac{\Theta}{2} \,. \tag{6.81}$$

This suggests the introduction of a dimensionless measure of the pathlength x,

$$\xi = N\pi a^2 \gamma x \,. \tag{6.82}$$

With this, (6.81) reduces to

$$-\frac{\mathrm{d}\epsilon}{\mathrm{d}\xi} = s(\epsilon) = \epsilon \int_0^\pi g\left(\epsilon, \sin^2 \frac{\Theta}{2}\right) \mathrm{d} \sin^2 \frac{\Theta}{2} \,. \tag{6.83}$$

This relation is general for elastic binary scattering on a screened-Coulomb potential in the nonrelativistic energy regime.

Specifically, with Lindhard-Scharff scaling, (6.57), this reduces to

$$\frac{\mathrm{d}\epsilon}{\mathrm{d}\xi} = \frac{1}{\epsilon} \int_0^\epsilon \mathrm{d}\eta \, f(\eta) \,, \tag{6.84}$$

where

$$\eta = \epsilon \sin^2 \frac{\Theta}{2} = \epsilon \frac{T}{\gamma E} \,, \tag{6.85}$$

and $f(\eta)$ is determined by the screening function of the potential.

Figure 6.22 shows $s_n(\epsilon)$ found by integration of the curves shown in Fig. 6.14 according to (6.84). In addition, the function

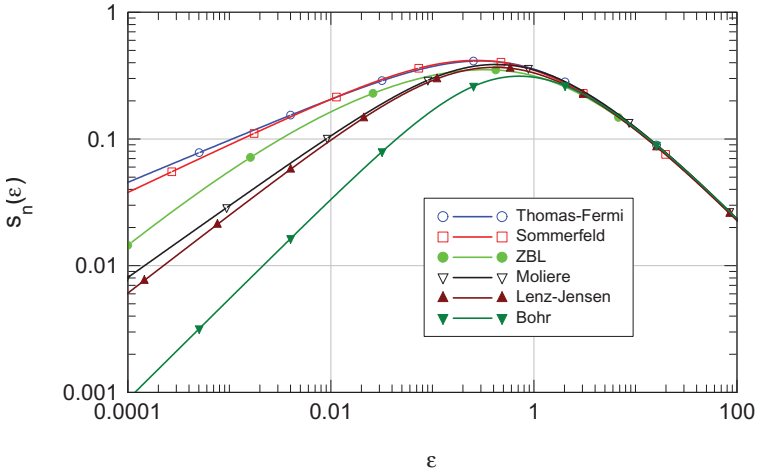

Fig. 6.22 Stopping cross sections in universal plot for the cross sections shown in Fig. 6.14. Also included is ZBL, i.e., the function adopted by Ziegler et al. (1985)

$$s_n = \frac{\ln(1 + a\epsilon)}{2(\epsilon + b\epsilon^c + d\sqrt{\epsilon})} \tag{6.86}$$

from Ziegler et al. (1985) with

$$a = 1.1383; \qquad b = 0.01321; \qquad c = 0.21226; \qquad d = 0.19593 \tag{6.87}$$

has been included. Note, however, that a comparison of the actual cross sections would have to take into account the adopted form of the screening radius.

6.4.2 Power Cross Section

Power cross sections have been introduced as a convenient tool in the derivation of the Lindhard-Scharff scaling relationship, (6.57). They have also been useful on their own as model cross sections in solving transport equations, as you will see in Chap. 9.

Going back to (6.57) and looking at Fig. 6.12 we may approximate $f(\eta)$ by

$$f_m(\eta) = \lambda_m \eta^{1-2m} \tag{6.88}$$

over a limited range of η-values, so that $m = 0$ yields a linear increase, applying to the low-η regime, while $m = 1$ characterizes the asymptotic behaviour at large η, i.e., Rutherford scattering.

Insertion of (6.88) into (6.57) yields

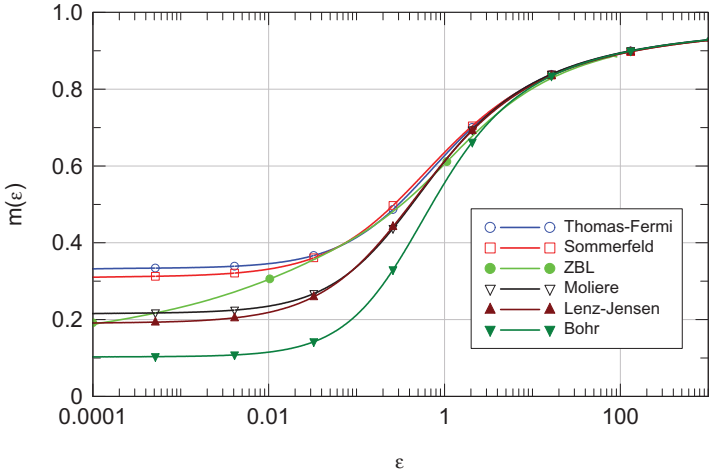

Fig. 6.23 Exponent m in power cross section extracted from stopping cross sections shown in Fig. 6.22

$$\mathrm{d}\sigma(E,T) = CE^{-m}T^{-1-m}dT \tag{6.89}$$

with

$$C = \frac{\pi}{2}\lambda_m a^2 \left(\frac{M_1}{M_2}\right)^m \left(\frac{2Z_1Z_2e^2}{a}\right)^{2m}, \tag{6.90}$$

where the numerical coefficient λ_m could be determined by going back to (6.23) and (6.50). It is, however, more efficient to determine λ_m by matching a power law to a more accurately determined scattering law. This could be either the function $f(\eta)$ or the stopping cross section. The latter takes the form

$$S = \int_0^{T_{\max}} T\,\mathrm{d}\sigma(E,T) = \frac{1}{1-m}C\gamma^{1-m}E^{1-2m}. \tag{6.91}$$

or, in dimensionless units,

$$s_n = \frac{\lambda_m}{2(1-m)}\epsilon^{1-2m}. \tag{6.92}$$

Figure 6.23 shows the variation of the exponent m found by matching the stopping cross sections shown in Fig. 6.22 in value and slope by the power form (6.91). You may note that there is a low-energy regime where a power law is a good approximation, and a high-energy regime close to Rutherford scattering.

The intermediate regime around $\epsilon \sim 1$ has frequently been characterized by $m = 1/2$ (Bohr, 1948, Nielsen, 1956, Firsov, 1958, Lindhard et al., 1963, Winterbon et al., 1970). Such a cross section is approximately equivalent with a potential $\propto 1/R^2$. Niels Bohr employed this potential to characterize the effect of 'excessive screening', i.e., interactions at distances $R \sim a$ and beyond. The corresponding

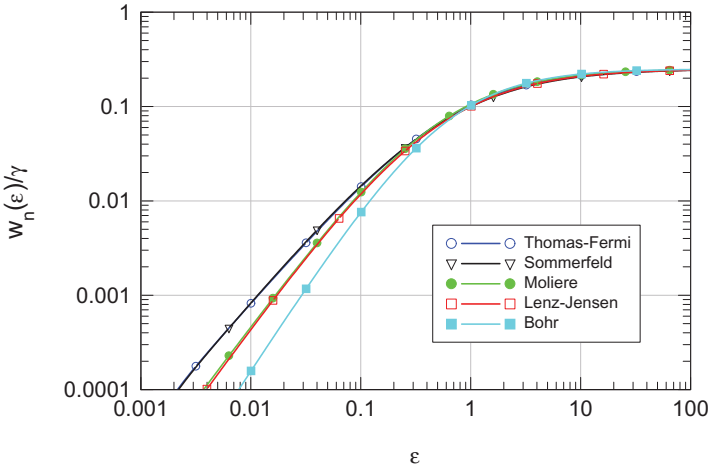

Fig. 6.24 Nuclear straggling in dimensionless units, (6.94)

differential cross section $\mathrm{d}\sigma(T) \propto \mathrm{d}T/T^{3/2}$ has convenient analytical properties. From (6.91) the particularly valuable property emerges that the stopping cross section becomes independent of energy for $m = 1/2$. The differential cross section expressed in the scattering angle becomes $\mathrm{d}\sigma(\Theta) \propto \mathrm{d}\Theta/\Theta^2$ at small angles. It will turn out that also this functional shape has convenient analytic properties.

The main drawback of the R^{-2} potential is that with its convenient analytic properties, numerous results can be derived that seemingly depend only on one parameter and frequently have the simple appearance of generally valid relationships. In other words, there is a temptation to ignore the limited range of validity of this particular interaction potential. This pitfall can be avoided with due care.

6.4.3 Straggling

The expression for straggling,

$$\frac{\mathrm{d}\Omega^2}{\mathrm{d}x} = \frac{\mathrm{d}}{\mathrm{d}x}\left\langle (\Delta E - \langle \Delta E\rangle)^2 \right\rangle = N \int T^2 \mathrm{d}\sigma(E,T) \tag{6.93}$$

may, for Lindhard-Scharff scaling, be written in the form

$$\frac{\mathrm{d}}{\mathrm{d}\xi}\left\langle (\Delta\epsilon - \langle \Delta\epsilon\rangle)^2 \right\rangle = w_n = \frac{\gamma}{\epsilon^2}\int_0^{\epsilon} \mathrm{d}\eta\, \eta^2 f(\eta)\,, \tag{6.94}$$

where according to (6.82)

$$\xi = N\pi a^2 \gamma x\,. \tag{6.95}$$

This is illustrated in Fig. 6.24 for the potentials shown in Fig. 6.14. This function approaches the value 1/4 at high energies (cf. Problem 6.8).

You may notice, by comparing Fig. 6.24 with Fig. 6.22, that $\sqrt{w_n}$ exceeds the stopping cross section s_n for $\epsilon > 1$. This is the regime where the differential cross section approaches the Rutherford cross section. If there were no electronic stopping, straggling would be governed by an analogue of the Landau distribution discussed in Sect. 9.3.2, Vol. 1.

6.4.4 Measurements of Nuclear Stopping

6.4.4.1 Experimental Aspects

Only a minute fraction of the experimental literature on stopping cross sections is devoted to nuclear stopping. This is by no means accidental.

Direct measurements of nuclear stopping have to take place at energies where electronic stopping is not dominating by several orders of magnitude, and accurate measurements require energies where nuclear stopping actually dominates. Even then, separating electronic from nuclear stopping is not a trivial task, as you will see in Chap. 7.

There are problems even in the absence of significant electronic stopping, which have been discussed in detail by Sidenius (1974):

- Nuclear energy loss is coupled to angular deflection. In the standard geometry the energy loss is measured in the beam direction with a narrow detection angle. Except for $M_1 \gg M_2$, ions with large energy losses will not be detected. While this simplifies the measurement of electronic stopping cross sections, nuclear stopping cross sections will be underestimated. Evidently, measurements of nuclear stopping require wide-angle detection. For $M_1 < M_2$ even detection in the backward direction may be necessary.
- In addition to beam particles the particle flux also contains energetic recoil atoms.

6.4.4.2 Results

In order to limit straggling to an acceptable limit, targets may have to be thin. Therefore, most direct measurements have been performed on gases.

Figure 6.25 shows measurements of Hvelplund (1975) with very heavy ions on hydrogen gas. The large mass ratio M_1/M_2 facilitates the detection of the entire scattered beam, and energies are low enough so that electronic stopping constitutes only a minor correction. Data for individual ions seem to fall on smooth curves which, by and large, lie in between the Thomas-Fermi and Lenz-Jensen predictions. Data for different ions differ significantly, more than what one would expect from universal scaling relations. Later time-of-flight data by Martini (1976) for the Pb-H_2 system (not shown in the graph) tend to agree with the data of Sidenius at the

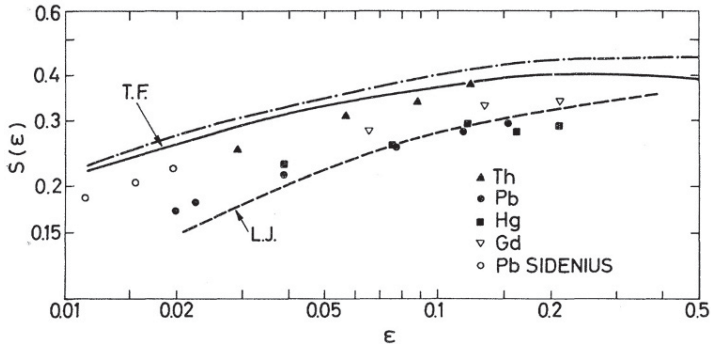

Fig. 6.25 Stopping cross section of heavy ions in hydrogen gas compared with theory. Data labelled Th, Pb, Hg and Gd: Stopping cross sections from Hvelplund (1975). Data labelled Sidenius from Sidenius (1963). Solid line: Thomas-Fermi nuclear stopping; dashed line: Lenz-Jensen nuclear stopping; dash-dotted curve: Total Thomas-Fermi stopping. From Hvelplund (1975)

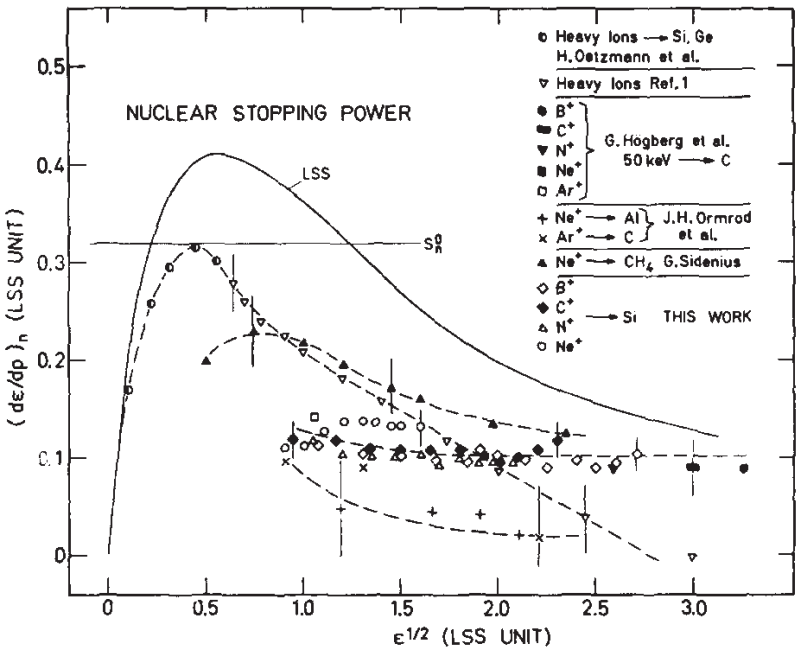

Fig. 6.26 Nuclear stopping cross section in Si. Comparison of various experimental results with universal stopping formula. See text. From Grahmann and Kalbitzer (1976)

low-energy end and with those of Hvelplund in the high-energy end. On the other hand, the difference between two data sets for Pb ions is as large as the difference between Th and Hg, suggesting that part of the deviation from scaling may be due to experimental error.

Figure 6.26 is another witness of the problematic nature of direct measurements of nuclear stopping. Experimental data for stopping of B, C, N, Ne and Ar ions in CH_4, C, Al, Si and Ge from several sources (Ormrod and Duckworth, 1963, Ormrod et al., 1965, Högberg and Skoog, 1972, Sidenius, 1974, Oetzmann et al., 1975, Grahmann and Kalbitzer, 1976) have been plotted in Lindhard-Scharff dimensionless units and compared with the Thomas-Fermi prediction of Lindhard et al. (1968). Apart from drastic deviations from the expected scaling behaviour you will notice that all experimental results lie significantly below the theoretical curve, even in the upper half of the abscissa variable, $\epsilon^{1/2} > 1.5$, where the stopping cross section should be independent of the adopted screening function according to Fig. 6.22.

What went wrong here? Firstly, data by Ormrod and Duckworth (1963), Ormrod et al. (1965), Högberg and Skoog (1972) had been taken with the aim of measuring electronic stopping. Nuclear stopping was minimized by choosing a detection angle that eliminated particles with a high nuclear energy loss. These data should not have been included in the graph. Secondly, data labelled 'this work' by Grahmann and Kalbitzer (1976) all refer to mass ratios $M_1/M_2 < 1$, where a noticeable fraction of the beam particles will suffer large-angle backscattering.

Conversely, the highest stopping cross sections listed in the graph refer to $M_1/M_2 > 1$ where this effect is much less pronounced. While the observed deviation from the Thomas-Fermi prediction fits well into the general pattern in the low-energy portion of the graph, the relatively small deviation found for the data of Sidenius (1974) can be ascribed to the fact that the target is CH_4, for which the scaling behaviour of atomic targets cannot be expected to be accurately fulfilled.

In brief, what remains of Fig. 6.26 is a scatter between relevant data of the same approximate magnitude as the one in Fig. 6.12, which serves as a theoretical basis for Lindhard-Scharff scaling.

The technique of Doppler-shift attenuation described briefly in Sect. 7.4.4, Vol. 1, has also been applied in low-energy stopping (Bister et al., 1975, Shane et al., 1976). While separation of nuclear from electronic stopping is not a trivial matter, comparisons with the Lindhard-Scharff predictions of the total stopping cross sections are much more favourable than what one might extract from Fig. 6.26.

6.5 Discussion and Outlook

The discussion in this chapter is based on Chap. 3, Vol. 1. Applications discussed there were dealing mainly with plain Coulomb interaction. Tools collected in the present chapter are quite adequate to treat scattering and nuclear stopping in the medium to upper keV regime and above. With equivalent knowledge of electronic stopping in this energy regime—to be discussed in Chap. 8—and suitable statistical tools—to be collected in Chap. 9—you will be well equipped to treat several aspects of particle penetration. Limitations prevail to lower energies especially in the medium and lower eV regime, where the many-body nature of collisions becomes exceedingly important, and where many-body potentials may be needed for quan-

titative predictions. These aspects become particularly important in the theory of radiation effects, the main subject of Volume 3 of this series.

Problems

6.1. Estimate the interaction potential between an ion 1 with a charge $q_1 e$ and a neutral atom 2 from the electrostatic interaction energy

$$\mathcal{V}(R) = -e \int \mathrm{d}^2 \boldsymbol{r}\, \rho_1(\boldsymbol{r}) \Phi_2(\boldsymbol{r}) \tag{6.96}$$

between two stiff charge distributions, characterized by potentials

$$\Phi_1(\boldsymbol{r}) = \frac{q_1 e}{r_1} + \frac{(Z_1 - q_1)e}{r_1} \mathrm{e}^{-r_1/a_1} \tag{6.97}$$

$$\Phi_2(\boldsymbol{r}) = \frac{Z_2 e}{r_2} \mathrm{e}^{-r_2/a_2}, \tag{6.98}$$

where r_1 and r_2 denote the distance from the respective nuclei, and a_1 and a_2 are arbitrary screening radii.

6.2. Figure 6.1 indicates that the screening function (6.5) turns negative at large values of R. Convince yourself, e.g. by looking at the limit $a_1/a_2 = 1$, that this is not a calculational error.

6.3. Consider a neutral Thomas-Fermi atom with a Yukawa-type charge density. Determine the kinetic energy per volume as well as the electrostatic energy per volume and compare the dependence on the distance r from the nucleus in the two cases. Show that regardless of atomic number and screening radius, electrostatic energy dominates at small r, while the opposite holds at large r.

6.4. Following Firsov (1957b) show that for a neutral system, the solution of the Thomas-Fermi equation minimizes the total energy. Hint: Set $\rho = \rho_0 + \delta\rho$, where ρ_0 is the charge density connected to an exact solution of the Thomas-Fermi equation for the potential. Insert this into (1.18) for $v = 0$ and expand in powers of $\delta\rho$. The zero-order term represents the exact energy, the linear term vanishes, and the quadratic term can be written in the form

$$\delta^2 \mathcal{E} = \frac{5}{9} \kappa_k \int \mathrm{d}^3 \boldsymbol{r}\, \frac{\delta\rho(\boldsymbol{r})^2}{\rho_0(\boldsymbol{r})^{1/3}} + \frac{e^2}{2} \int \mathrm{d}^3 \boldsymbol{r}\, \mathrm{d}^3 \boldsymbol{r}' \frac{\delta\rho(\boldsymbol{r}) \delta\rho(\boldsymbol{r}')}{|\boldsymbol{r} - \boldsymbol{r}'|}, \tag{6.99}$$

which is positive.

6.5. By solving Problem 3.8, Vol. 1, you will arrive at the scattering law for a Bohr potential, (6.32),

$$\Theta(p) = \frac{2Z_1Z_2}{m_0v^2} K_1\left(\frac{p}{a}\right) \tag{6.100}$$

for small scattering angles, where K_1 denotes a modified Bessel function in standard notation (Abramowitz and Stegun, 1964). Evaluate (6.31) for this scattering law.

Write the result in the form

$$\frac{2Z_1Z_2e^2}{\hbar v} \gg g_2(p/a), \tag{6.101}$$

and demonstrate that $g_2(p/a) \equiv 1$ for unscreened Coulomb interaction.

6.6. Khodyrev (2000) argues that the Bohr criterion (6.24) ought to be replaced by

$$2p \gg \lambda\!\!\!^{-}. \tag{6.102}$$

Identify the difference to Bohr's argument, and try to form an opinion on what is most relevant.

6.7. Problem 3.6, Vol. 1, concerns the scattering integral for the potential $\mathcal{V}(R) = A/R^2$, where A is a constant. Use the solution of that problem, $\Theta = \pi(1 - p/\sqrt{p^2 + A/E_r})$, to derive the potential by means of the Firsov inversion formula, (6.69).

6.8. Show that for Rutherford scattering, the function $w(\epsilon)/\gamma$ shown in Fig. 6.24 reduces to $w(\epsilon)/\gamma \equiv 1/4$.

References

Aberth W., Lorents D.C., Marchi R.P. and Smith F.T. (1965): Effect of nuclear symmetry in ion-atom scattering. Phys Rev Lett **14**, 776–778

Abrahamson A.A. (1963a): Repulsive interaction potentials between rare-gas atoms. heteronuclear two-center systems. Phys Rev **133**, A990–A1004

Abrahamson A.A. (1963b): Repulsive interaction potentials between rare-gas atoms. homonuclear two-center systems. Phys Rev **130**, 693–707

Abrahamson A.A., Hatcher R.D. and Vineyard G.H. (1961): Interatomic repulsive potentials at very small and intermediate separations. Phys Rev **121**, 159–171

Abramowitz M. and Stegun I.A. (1964): *Handbook of mathematical functions*. Dover, New York

Adams J.B. and Foiles S.M. (1990): Development of an embedded-atom potential for a bcc metal: Vanadium. Phys Rev B **41**, 3316–3328

Afrosimov V.V., Gordeev Y.S., Nikulin V.K., Polyanski A.M. and Shergin A.P. (1972): Singularities in scattering of atomic particles in collisions involving the excitation of inner electron shells. Zh Exp Teor Fiz **62**, 848–862. [Engl. Transl. in Sov. Phys. JETP 35, 449-456 (1972)]

Amdur I. and Mason E.A. (1956): Scattering of high velocity neutral particles .IX. Ne-A; A-Ne. J Chem Phys **25**, 632–634

Biersack J.P. and Ziegler J.F. (1982): Refined universal potentials in atomic collisions. Nucl Instrum Methods **194**, 93–100

Bister M., Anttila A. and Keinonen J. (1975): Method for determination of nuclear and electronic stopping power parameters. Phys Lett A **53**, 471–472

Bohr N. (1948): The penetration of atomic particles through matter. Mat Fys Medd Dan Vid Selsk **18 no. 8**, 1–144

Born M. and Mayer J.E. (1932): Zur Gittertheorie der Ionenkristalle. Physica B **75**, 1–18

Daw M.S. (1989): Model of metallic cohesion: The embedded-atom method. Phys Rev B **39**, 7441

Daw M.S. and Baskes M.I. (1983): Semiempirical, quantum-mechanical calculation of hydrogen embrittlement in metals. Phys Rev Lett **50**, 1285

Daw M.S. and Baskes M.I. (1984): Embedded-atom method – derivation and application to impurities, surfaces, and other defects in metals. Phys Rev B **29**, 6443–6453

Dedkov G.V. (1984): On the theory of the interatomic interaction potential at high projectile velocities. Radiat Eff Lett **86**, 127–132

Dedkov G.V. (1989): Interatomic interaction potentials in the electron gas approximation: Static case. Nucl Instrum Methods B **36**, 14–22

Dedkov G.V. (1995): The interatomic interaction potentials in radiation physics. phys stat sol A **149**, 453–514

Demkov Y.N., Ostrovskii V.N. and Berezina N.B. (1971): Uniqueness of the Firsov inversion method and focusing potentials. Zh Eks Teor Fiz **60**, 1604–1610. [Engl. Transl. in Sov. Phys. JETP 33, 867-870]

Everhart E., Carbone R.J. and Stone G. (1955): Differential cross-section measurements for large-angle collisions of helium, neon and argon ions with argon atoms at energies to 100 keV. Phys Rev **98**, 1045–1049

Fermi E. and Amaldi E. (1934): Le orbite degli elementi. Mem Accad Italia **6**, 119–149

Firsov O.B. (1953): Opredelenie sil, deistvuyushchikh mezhdu atomami, pri pomoshchi differentsialnogo effektivnogo secheniya uprugogo rasseyaniya. Zh Eksp Teor Fiz **24**, 279

Firsov O.B. (1957a): Calculation of the interaction potential of atoms. Zh Eksp Teor Fiz **33**, 696. [Engl. transl. Sov. Phys. JETP 6, 5340-537 (1958)]

Firsov O.B. (1957b): Interaction energy of atoms for small nuclear separations. Zh Eksp Teor Fiz **32**, 1464–1469. [Engl. transl. Sov. Phys. JETP **5**, 1192-1196(1957)]

Firsov O.B. (1958): Scattering of ions by atoms. Zh Eksp Teor Fiz **34**, 447. [Engl. transl. Soviet Physics Jetp 7, 308-311 (1958)]

Gilbert T.L. and Wahl A.C. (1967): Single-configuration wavefunctions and potential curves for ground states of He_2, Ne_2 and Ar_2. J Chem Phys **47**, 3425–

Gombas P. (1949): *Die Statistische Theorie des Atoms*. Springer, Vienna

Grahmann H. and Kalbitzer S. (1976): Nuclear and electronic stopping powers of low energy ions with $Z \leq 10$ in silicon. Nucl Instrum Methods **132**, 119–123

Günther K. (1964): Über die Existenz eines Maximalprinzips als äquivalente Formulierung des Thomas-Fermi-Dirac-Modells und das TFD-Wechselwirkungspotential v on Atomen. Ann Physik **14**, 296–309

Hartree D.R. and Hartree W. (1938): Self-consistent field with exchange for potassium and argon. Rev Mod Phys **166**, 450–464

Hartung H., Fricke B., Sepp W.D., Sengler W. and Kolb D. (1985): Theoretical evidence for quasi-molecular structure at small internuclear distances in elastic ion-atom scattering. J Phys B **18**, L433–L437

Herman F. and Skillman S. (1963): *Atomic structure calculations*. Prentice Hall, New Jersey

Högberg G. and Skoog R. (1972): Non-evidence for Z_1 oscillations of the nuclear ion-atom interaction in an amorphous target. Radiat Eff **13**, 197–202

Hoyt F.C. (1939): The determination of force fields from scattering in the classical theory. Phys Rev **55**, 664–665

Hvelplund P. (1975): Energy loss and straggling of 100-500 keV $_{90}$Th, $_{82}$Pb, $_{80}$Hg, and $_{64}$Gd in H_2. Phys Rev A **11**, 1921–1927

Jensen H. (1932): Die Ladungsverteilung in Ionen und die Gitterkonstante des Rubidiumbromids nach der statistischen Methode. Z Physik **77**, 722

Kaminker D.M. and Fedorenko N.V. (1955): Single scatter of argon ions during stripping in a gas. Zh Tekh Fiz **25**, 2239–2255

Khodyrev V.A. (2000): On the origin of the Bloch correction in stopping. J Phys B **33**, 5045–5056

Kim Y.S. and Gordon R.G. (1974): Ionrare gas interactions on the repulsive part of the potential curves. J Chem Phys **60**, 4323–4331

Klein O. (1932): Zur Berechnung von Potentialkurven für zweiatomige Moleküle mit Hilfe von Spektraltermen. Z Physik **76**, 226–235

Kuzmin V. (2006): Range parameters of heavy ions in carbon calculated with first-principles potentials. Nucl Instrum Methods B **249**, 13–17

Lane G.H. and Everhart E. (1960): Ion-atom potential functions obtained from keV scattering data. Phys Rev **120**, 2064–

Lennard-Jones J.E. (1924): On the determination of molecular fields. Proc Roy Soc A **106**, 463–477

Lenz W. (1932): Über die Anwendbarkeit der statistischen Methode auf Ionengitter. Z Physik **77**, 713

Lindhard J. (1965): Influence of crystal lattice on motion of energetic charged particles. Mat Fys Medd Dan Vid Selsk **34 no. 14**, 1–64

Lindhard J., Nielsen V. and Scharff M. (1968): Approximation method in classical scattering by screened Coulomb fields. Mat Fys Medd Dan Vid Selsk **36 no. 10**, 1–32

Lindhard J., Scharff M. and Schiøtt H.E. (1963): Range concepts and heavy ion ranges. Mat Fys Medd Dan Vid Selsk **33 no. 14**, 1–42

Lockwood G.J., Helbig H.F. and Everhart E. (1963): Measurements of resonant electron capture in He^+ on He collisions. Phys Rev **132**, 2078–2082

Loftager P., Besenbacher F., Jensen O.S. and Sørensen V.S. (1979): Experimental study of effective interaction potentials. Phys Rev A **20**, 1443

Loftager P. and Hermann G. (1968): Influence of Q values in atomic single collisions on observed scattering cross sections and som Q values. Phys Rev Lett **21**, 1623–1626

Martini V. (1976): Stopping cross-section measurements with heavy ions in keV energy-range in gases by time-of-flight spectroscopy. Nucl Instrum Methods **139**, 163–167

Molière G. (1947): Theorie der Streuung schneller geladener Teilchen I. Einzelstreuung am abgeschirmten Coulomb-Feld. Z Naturforsch **2a**, 133–145

Nielsen K.O. (1956): The range of atomic particles with energies about 50 keV. In M.L. Smith, editor, *Electromagnetically Enriched Isotopes and Mass Spectrometry*. AERE Harwell, Butterworth Sci. Pub., London

Nikulin V.K. (1971): Calculation of repulsive atomic-interaction potentials from statistical theory. Zh Tekh Fiz **41**, 33–40. [Engl. transl.: Sov. Phys. Techn. Phys. 16, 21-27 (1971)]

Nørskov J.K. (1977): Electronic structure of H and He in metal vacancies. Sol St Comm **24**, 691–693

Nørskov J.K. (1982): Covalent effects in the effective-medium theory of chemical binding: Hydrogen heats of solution in the 3d metals. Phys Rev B **26**, 2875–2885

Nørskov J.K. and Lang N.D. (1980): Effective-medium theory of chemical binding: Application to chemisorption. Phys Rev B **21**, 2131–2136

Oen O.S. (1983): Universal shadow cone expressions for an atom in an ion-beam. Surf Sci **131**, L407–L411

Oetzmann H., Feuerstein A., Grahmann H. and Kalbitzer S. (1975): Range parameters of heavy-ions in amorphous targets at LSS-energies of $0.0006 \leq \epsilon \leq 0.3$. Phys Lett A **55**, 170–172

Olsen J.O., Andersen T., Barat M., Courbin-Gaussorgues C., Sidis V., Pommier J., Agusti J., Andersen N. and Russek A. (1979): Excitation and charge transfer in low-energy Na^+-Ne collisions. Phys Rev A **19**, 1457–1484

Ormrod J.H. and Duckworth H.E. (1963): Stopping cross sections in carbon for low-energy atoms with $Z \leq 12$. Can J Physics **41**, 1424–1442

Ormrod J.H., MacDonald J.R. and Duckworth H.E. (1965): Some low-energy atomic stopping cross sections. Can J Physics **43**, 275–284

Robinson M.T. (1970): Table of classical scattering integrals. Tech. Rep. ORNL-4556, Oak Ridge National Laboratory

Shane K.C., Laumer H. and Seaman G.G. (1976): Energy loss of low-energy ^{40}Ca ions in C. J Appl Phys **47**, 2286–2288

Sidenius G. (1963): In M.R.C. McDowell, editor, *Proceedings of the 3rd International Conference on Atomic Collisions*, 709. North Holland, Amsterdam

Sidenius G. (1974): Systematic stopping cross section measurements with low energy ions in gases. Mat Fys Medd Dan Vid Selsk **39 no. 4**, 1–32

Sigmund P. (1997): Charge-dependent electronic stopping of swift nonrelativistic heavy ions. Phys Rev A **56**, 3781–3793

Srivastava K.P. (1958): Unlike molecular interactions and properties of gas mixtures. J Chem Phys **28**, 543–549

Stillinger F.H. and Weber T.A. (1985): Computer simulation of local order in condensed phases of silicon. Phys Rev B **31**, 5262–5271

Stott M.J. and Zaremba E. (1980): Quasiatoms: An approach to atoms in nonuniform electron systems. Phys Rev B **22**, 1564–1583

Tersoff J. (1986): New empirical model for the structural properties of silicon. Phys Rev Lett **56**, 632–635

Wedepohl P.T. (1967): Influence of electron distribution on atomic interaction potentials. Proc Phys Soc **92**, 79–93

Wilson W.D. and Bisson C.L. (1971): Inert gases in solids: Interatomic potentials and their influence on rare-gas mobility. Phys Rev B **3**, 3984–3992

Wilson W.D., Haggmark L.G. and Biersack J.P. (1977): Calculations of nuclear stopping, ranges and straggling in the low-energy region. Phys Rev B **15**, 2458–2468

Winterbon K.B. (1972): Heavy-ion range profiles and associated damage distributions. Radiat Eff **13**, 215–226

Winterbon K.B., Sigmund P. and Sanders J.B. (1970): Spatial distribution of energy deposited by atomic particles in elastic collisions. Mat Fys Medd Dan Vid Selsk **37 no. 14**, 1–73

Witte H. and Wölfel E. (1958): Electron distributions in NaCl, LiF, CaF_2, and Al. Rev Mod Phys **30**, 51–55

Yamamura Y. and Takeuchi W. (1984): Large-angle surface scattering of low-energy ions in the 2-atom scattering model. Radiat Eff **82**, 73–84

Ziegler J.F., Biersack J.P. and Littmark U. (1985): *The stopping and range of ions in solids*, vol. 1 of *The stopping and ranges of ions in matter*. Pergamon, New York

Ziemba F.P. and Everhart E. (1959): Resonance phenomena in large-angle helium ion-helium atom collisions. Phys Rev Lett **2**, 299–301

Zinoviev A.N. (2011): Interaction potentials for modeling of ion-surface scattering. Nucl Instrum Methods B **269**, 829–833